An Ideal Molecular Sieve for Acetylene Removal from Ethylene with Record Selectivity and Productivity

Bin Li, Xili Cui, Daniel O'Nolan, Hui-Min Wen, Mengdie Jiang, Rajamani Krishna, Hui Wu, Rui-Biao Lin, Yu-Sheng Chen, Daqiang Yuan, Huabin Xing,* Wei Zhou,* Qilong Ren, Guodong Qian, Michael J. Zaworotko,* and Banglin Chen*

Realization of ideal molecular sieves, in which the larger gas molecules are completely blocked without sacrificing high adsorption capacities of the preferred smaller gas molecules, can significantly reduce energy costs for gas separation and purification and thus facilitate a possible technological transformation from the traditional energy-intensive cryogenic distillation to the energy-efficient, adsorbent-based separation and purification in the future. Although extensive research endeavors are pursued to target ideal molecular sieves among diverse porous materials, over the past several decades, ideal molecular sieves for the separation and purification of light hydrocarbons are rarely realized. Herein, an ideal porous material, SIFSIX-14-Cu-i (also termed as UTSA-200), is reported with ultrafine tuning of pore size (3.4 Å) to effectively block ethylene (C_2H_4) molecules but to take up a record-high amount of acetylene (C_2H_2, 58 cm^3 cm^{-3} under 0.01 bar and 298 K). The material therefore sets up new benchmarks for both the adsorption capacity and selectivity, and thus provides a record purification capacity for the removal of trace C_2H_2 from C_2H_4 with 1.18 mmol g^{-1} C_2H_2 uptake capacity from a 1/99 C_2H_2/C_2H_4 mixture to produce 99.9999% pure C_2H_4 (much higher than the acceptable purity of 99.996% for polymer-grade C_2H_4), as demonstrated by experimental breakthrough curves.

Porous materials offer promise for the separation and purification of industrial commodity chemicals through adsorbent- and/or membrane-based separation technologies and thus might enable a transition from established separation technologies such as cryogenic distillation, which currently accounts for 10–15% of the world's energy consumption.[1–4] Although such promise has not been fully fulfilled, extensive research efforts have indeed led to progress over the past several decades. For example, the discovery of the molecular gate adsorbent ETS-4 has initiated the industrial scale nature gas separation.[5,6]

Pore tuning and pore functionalization are two powerful approaches to introduce molecular sieving and preferential binding effects and thus are very important to target porous materials for the efficient gas separation and purification, as clearly demonstrated in ETS-4 series and zeolite LiX materials for CH_4/N_2 and N_2/O_2 separations, respectively.[5,7] Whereas

Dr. B. Li, Prof. G. Qian, Prof. B. Chen
State Key Laboratory of Silicon Materials
Cyrus Tang Center for Sensor Materials and Applications
School of Materials Science and Engineering
Zhejiang University
Hangzhou 310027, China
E-mail: banglin.chen@utsa.edu
Dr. X. Cui, M. Jiang, Prof. H. Xing, Prof. Q. Ren
Key Laboratory of Biomass Chemical Engineering
of Ministry of Education
College of Chemical and Biological Engineering
Zhejiang University
Hangzhou 310027, China
E-mail: xinghb@zju.edu.cn
D. O'Nolan, Prof. M. J. Zaworotko
Bernal Institute, Department of Chemical Sciences
University of Limerick
Limerick, V94 T9PX, Republic of Ireland
E-mail: michael.zaworotko@ul.ie

The ORCID identification number(s) for the author(s) of this article can be found under https://doi.org/10.1002/adma.201704210.

Dr. H.-M. Wen, Dr. R.-B. Lin, Prof. B. Chen
Department of Chemistry
University of Texas at San Antonio
One UTSA Circle, San Antonio, TX 78249-0698, USA
Prof. R. Krishna
Van't Hoff Institute for Molecular Sciences
University of Amsterdam
Science Park 904, 1098 XH Amsterdam, Netherlands
Dr. H. Wu, Dr. W. Zhou
NIST Center for Neutron Research
National Institute of Standards and Technology
Gaithersburg, MD 20899-6102, USA
E-mail: wzhou@nist.gov
Dr. Y.-S. Chen
ChemMatCARS
Center for Advanced Radiation Sources
The University of Chicago
9700 South Cass Avenue, Argonne, IL 60439, USA
Prof. D. Yuan
State Key Laboratory of Structure Chemistry
Fujian Institute of Research on the Structure of Matter
Chinese Academy of Sciences
Fuzhou, Fujian 350002, China

traditional zeolite-type materials are quite limited in terms of tuning pore size and functionalization, basically through control of the thermal activation and substitutions of metal cations, microporous metal–organic frameworks, and related classes of materials have provided us the rich chemistry to realize fine pore tuning and functionalization, and thus target materials for gas separation and purification through the judicial choices of metal clusters and organic linkers, framework topology design, framework interpenetration control, and immobilization of specific functional sites.[8–16] Indeed, a number of microporous metal–organic frameworks (MOFs) have been realized to address a diverse range of gas separations over the past decades through a synergistic approach to pore tuning and functionalization.[17–27] Recent progress on this topic for the separation of C_2H_2/C_2H_4 and C_3H_6/C_3H_8 is of particularly interest.[28,29] In the former case of SIFSIX-2-Cu-i, the trade-off between adsorption capacity and selectivity for separating the challenging gas mixtures of C_2H_2/C_2H_4 has been significantly minimized; in the latter case, NbOFFIVE-1-Ni exhibits a molecular sieving effect for C_3H_6/C_3H_8 separation. Although these two porous materials exhibit benchmark performance for the above-mentioned gas separations, they still suffer from certain degree of the trade-off effects: the C_2H_2/C_2H_4 selectivity (S_{ac}) of SIFSIX-2-Cu-i does not preclude coadsorption of the larger molecule, C_2H_4, when C_2H_2 is a minor impurity; NbOFFIVE-1-Ni can adsorb small amounts of the smaller molecule of C_3H_6, particularly under low pressure of 0.1 bar ($\approx$5.3 cm^3 g^{-1}), deviating from the ideal molecular sieves (ideal molecular sieves are defined as those which can completely block the larger gas

molecules and take up large amount of the smaller gas molecules from gas mixtures). Realization of ideal molecular sieves can certainly enable ultrahigh selectivity and working capacity for diverse gas separations and thus improve the product purity and adsorbent productivity in the adsorption-based separation process that is driven by pressure swing adsorption, thermal swing adsorption, or membrane-based operations, to result in the significant energy savings.[30–35] To the best of our knowledge, there are only a few reported molecular sieves for carbon capture and separation of olefin/paraffin.[29,36–41] We target this matter herein through the study of SIFSIX-14-Cu-i (UTSA-200), a new variant of SIFSIX-2-Cu-i, to realize the ideal molecular sieve for separation and purification of C_2H_2/C_2H_4 mixtures with the record selectivity and C_2H_4 productivity ever reported.

Structural and modeling studies have indicated that the pores of about 4.4 Å in SIFSIX-2-Cu-i remain slightly larger than the size of C_2H_4 (kinetic dimensions 4.2 Å)[42] and thus cannot exhibit a sieving effect for C_2H_4 (Figure S3, Supporting Information). We speculated that if a shorter organic linker of 4,4′-azopyridine (azpy, 9.0 Å) instead of 4,4′-dipyridylacetylene (dpa, 9.6 Å) is used to construct the isoreticular SIFSIX-14-Cu-i /UTSA-200 (**Figure 1**), the resulting microporous material was expected to exhibit a smaller pore size of ≈3.3–4.0 Å that might completely block C_2H_4 molecules while enhance the affinity of the functional SiF$_6^{2-}$ sites toward C_2H_2, thus targeting an ideal molecular sieve for the extremely highly efficient removal of C_2H_2 from a 1/99 C_2H_2/C_2H_4 mixture to produce high purity of C_2H_4 in a much higher production scale than SIFSIX-2-Cu-i. Our experimental and simulation studies verify this hypothesis,
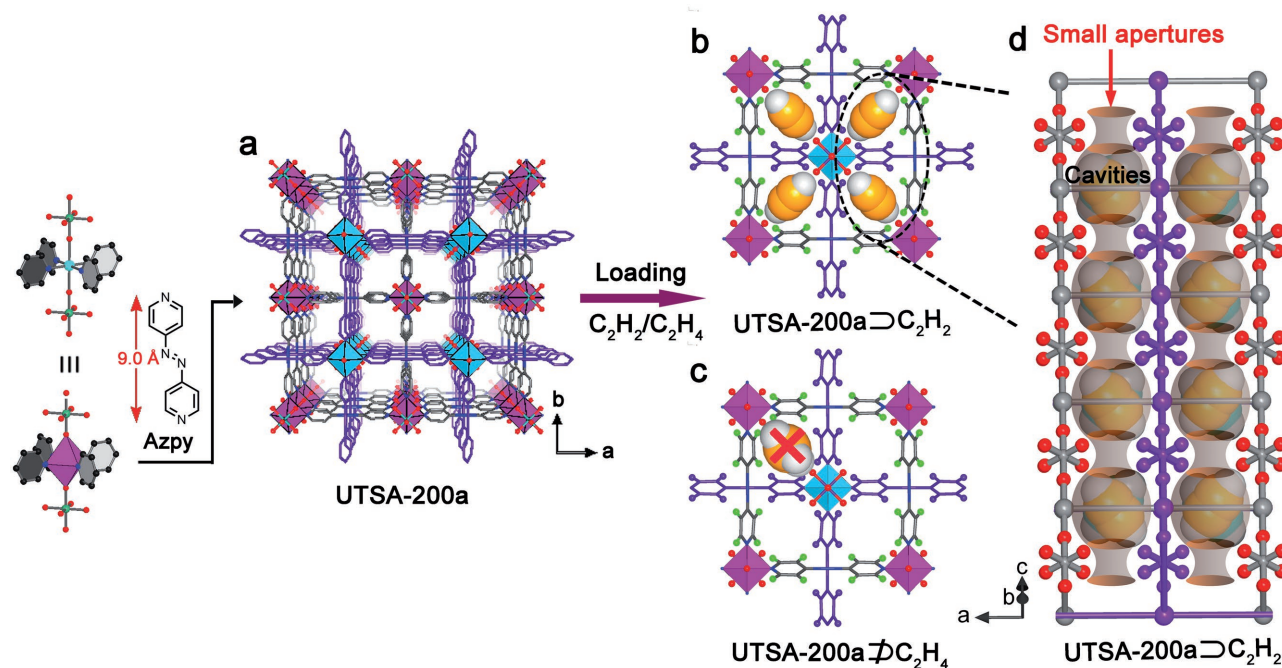
Figure 1. Structure description of UTSA-200a. a) The channel structure of UTSA-200a reveals a pores size of ≈3.4 Å. b) DFT-D-calculated C_2H_2 adsorption models in UTSA-200a, revealing that this pore size enables the passage of C_2H_2 molecules. c) Simulated C_2H_4 adsorption in UTSA-200a indicating that the C_2H_4 molecule are too large to pass through the pores. d) Schematic illustration of ideal molecular sieves based on the structure of UTSA-200a⊃C_2H_2, in which larger cavities suitable for strongly binding C_2H_2 molecules are interconnected by narrow apertures that serve as sieves for C_2H_4 but not for C_2H_2. The different nets are highlighted in gray and purple for clarity. Color code: Cu (turquoise), Si (dark green), F (red), N (blue), C (gray), and H (green spheres).

and we report herein the structure, adsorption isotherms, simulated and experimental breakthrough curves of SIFSIX-14-Cu-i (UTSA-200). These data reveal that SIFSIX-14-Cu-i (UTSA-200) is the new benchmark porous material for the removal of C_2H_2 from C_2H_4 in a 1/99 mixture that mimics that present in large-scale industrial ethylene production processes.

Reaction of azpy with $CuSiF_6$ afforded saffron prism-shaped crystals of $[Cu(azpy)_2(SiF_6)]_n$ (see the Supporting Information for synthetic and crystallographic details). The single-crystal X-ray diffraction analysis revealed that UTSA-200 has doubly interpenetrated nets that are isostructural to the nets in SIFSIX-2-Cu-i.[18] After removing guest molecules, we further collected the desolvated structure, that is, UTSA-200a, by using neutron powder diffraction experiments at 200 K. As revealed by Figure 1a, the use of the shorter azpy instead of dpa as a linker offers: (i) a commensurate reduction on the pore size; and (ii) a certain degree of tilting of the pyridine moieties, which are rotated by around 28 degrees with respect to the crystal axis (Figure S4, Supporting Information). The SiF_6^{2-} pillars and pyridine rings are interconnected through a strong hydrogen bonding of $C-H\cdots F$ (2.326 Å) to restrict the rotation of pyridine rings. This tilt of pyridine rings thereby results in the pore size of UTSA-200a being notably reduced to 3.4 Å. In addition, the channels of UTSA-200a exhibit the features of ideal molecular sieves, in which larger cavities functionalized with the SiF_6^{2-} binding sites are interconnected by narrow apertures of 3.4 Å (molecular sieving dimension, Figure 1d; Figure S5, Supporting Information). This narrow aperture size was further confirmed by the calculated pore size distributions, where the pore sizes of UTSA-200a are less than 3.6 Å (Figure S6, Supporting Information), in good agreement with the results of structural analysis. We note that the aperture size of 3.4 Å is much smaller than the kinetic diameter of C_2H_4 molecule (4.2 Å) but slightly larger than that of C_2H_2 (3.3 Å), consistent with the potential for selective molecular sieving in C_2H_2/C_2H_4 separations.

We first performed detailed modeling studies using first-principles dispersion-corrected density functional theory (DFT-D) method on UTSA-200a and compared the results with SIFSIX-2-Cu-i to evaluate the possible sieving effect on C_2H_2/C_2H_4 molecules. In the 2-fold interpenetrated structure of SIFSIX-2-Cu-i, the window size of 4.4 Å is larger than both C_2H_2 and C_2H_4, thereby allowing both C_2H_2 and C_2H_4 molecules to enter the cavities (Figure S3, Supporting Information). Each adsorbed C_2H_2 or C_2H_4 molecule is simultaneously bound by two SiF_6^{2-} sites from different nets through cooperative $C-H\cdots F$ H-bonding (2.015 Å for C_2H_2 and 2.186 Å for C_2H_4).[28] When the aperture size was reduced to 3.4 Å in UTSA-200a, our computational results indicated that the contracted aperture size still allows C_2H_2 molecules to enter the pore cavities and bind in the same fashion upon adsorption (Figure 1b). The calculated distance of $C-H\cdots F$ H-bonding in UTSA-200a is shorter (1.900 Å) than that in SIFSIX-2-Cu-i (Figure S7, Supporting Information). In contrast, when loading a C_2H_4 molecule into the pores, we found that the C_2H_4 molecule would have inevitable space overlapping with the pore walls of UTSA-200a (Figure 1c), suggesting that the size of C_2H_4 may mismatch with the host framework and thereby to be size excluded. These calculated studies support that the

contracted pore size of UTSA-200a (vs SIFSIX-2-Cu-i) might enable sieving of C_2H_2 from C_2H_4.

The performance of UTSA-200a was determined by examining its gas sorption and separation properties. As illustrated in **Figure 2**a, UTSA-200a exhibits almost no N_2 uptake at 77 K, indicating that even N_2 (3.64 Å) is blocked at this low cryogenic temperature because of the small aperture size. On the other hand, for CO_2 (kinetic diameter 3.3 Å), a high amount of CO_2 is absorbed (153 cm^3 g^{-1}) at 196 K and 1 bar with type I sorption behavior characteristic of microporous materials. The Brunauer–Emmett–Teller (BET) surface area and pore volume were calculated to be 612 m^2 g^{-1} and 0.27 cm^3 g^{-1}, respectively, slightly lower than SIFSIX-2-Cu-i (735 m^2 g^{-1} and 0.31 cm^3 g^{-1}).

Pure component equilibrium adsorption isotherms for C_2H_2 and C_2H_4 were measured at 298 K up to 1 bar, as presented in Figure 2b. Detailed analysis revealed that UTSA-200a exhibits a steep and high C_2H_2 uptake of 116 cm^3 cm^{-3} at 298 K and 1 bar. This value is comparable to the uptake of SIFSIX-2-Cu-i and is expected thanks to their similar pore chemistry. However, contraction of pore size in UTSA-200a was found to enable higher uptake than SIFSIX-2-Cu-i within the low pressure of 0.025 bar (Figure 2c). At 0.01 bar, which is an indicator of the C_2H_2 capture ability of adsorbents from a C_2H_2/C_2H_4 mixture (1/99, v/v), UTSA-200a exhibits notably enhanced C_2H_2 uptake (58 cm^3 cm^{-3}) versus SIFSIX-2-Cu-i (42 cm^3 cm^{-3}). In comparison to other top-performing materials, UTSA-200a exhibits a new benchmark for C_2H_2 uptake at 0.01 bar (Figure 2d), even higher than Mg- and Fe-MOF-74, indicating its ultrastrong C_2H_2 capture capacity at low pressure. Conversely, as revealed by Figure 2b, the smaller static pore size of UTSA-200a can completely prevent the entrance of C_2H_4 molecule below 0.2 bar and has very little uptake ($\approx$0.25 mmol g^{-1}) up to 0.7 bar at 298 K, which is dramatically lower than that of SIFSIX-2-Cu-i (2.28 mmol g^{-1}). When the pressure was further increased to 1 bar, C_2H_4 adsorption isotherm slopes up. This is because the N=N bond and the pyridine rings in the MOF linker have certain rotational flexibility, so the pore sizes were slightly enlarged under higher pressure (larger than 0.7 bar) to take up small amount of C_2H_4 molecules (Figure S8, Supporting Information). Nevertheless, the C_2H_4 uptake amounts of UTSA-200a in the entire range of 1 bar are still the lowest among the indicated materials (Figure S9, Supporting Information). Therefore, our adsorption findings demonstrated that the contracted pore size of UTSA-200a supports to efficiently block C_2H_4 molecules without sacrificing its high C_2H_2 adsorption capacity, rendering UTSA-200a an ideal candidate for C_2H_2/C_2H_4 separation at ambient conditions.

To gain further insight into the ultrastrong C_2H_2 adsorption and confirm the calculated C_2H_2 binding sites, high-resolution neutron powder diffraction data were collected on C_2D_2-loaded samples of UTSA-200a and Rietveld structural refinements were conducted (Figure S11, Supporting Information). After the samples loaded with various amount of C_2D_2 molecules, the MOF lattice can be slightly distorted from the tetragonal symmetry to a monoclinic lattice. As shown in Figure 2e,f, each adsorbed C_2D_2 molecule interacts with two SiF_6^{2-} anions from different nets through cooperative $C-D\cdots F$ H-bonding, which is consistent well with the previous calculated C_2H_2 binding configuration. Because of the smaller pore size, the
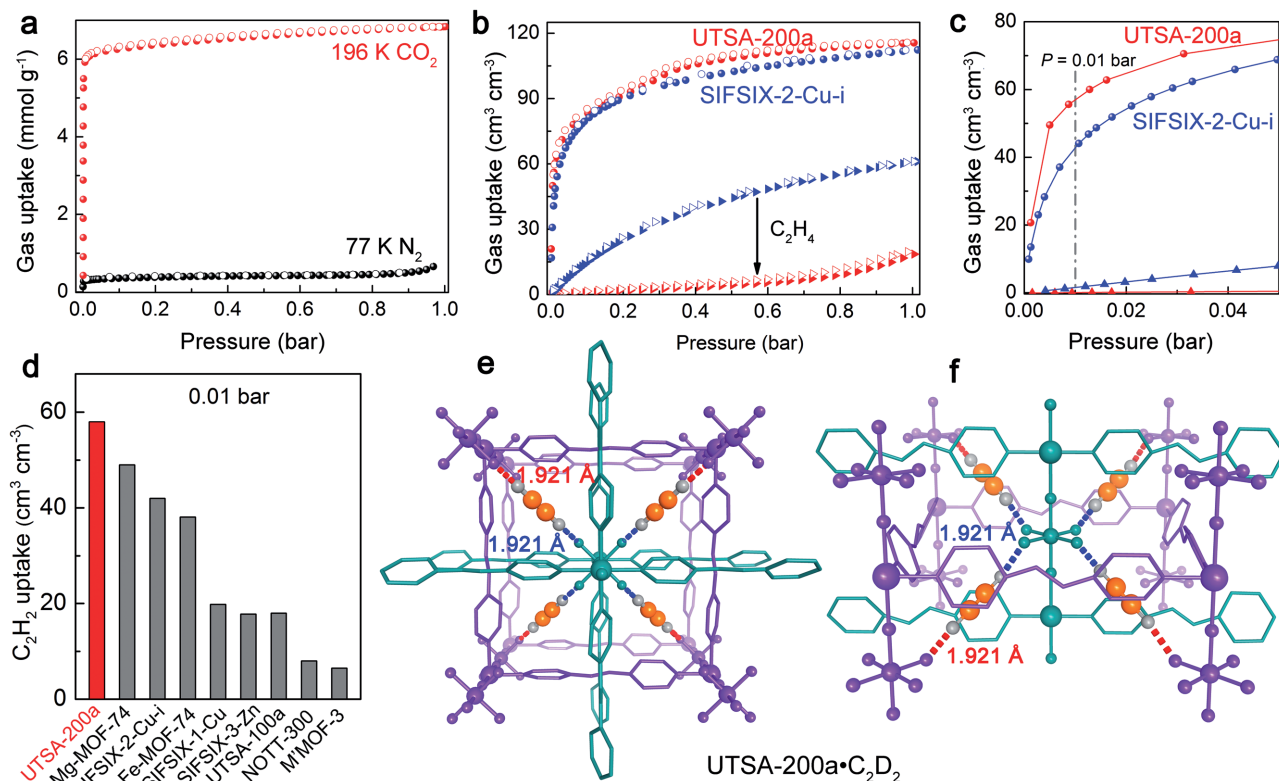
Figure 2. Gas adsorption isotherms and neutron crystal structure of UTSA-200a·C_2D_2. a) Gas adsorption isotherms of UTSA-200a for CO_2 at 196 K and N_2 at 77 K. Adsorption isotherms of C_2H_2 (circles) and C_2H_4 (triangles) for UTSA-200a and SIFSIX-2-Cu-i at 298 K in two pressure regions, b) 0–1.0 bar and c) 0–0.05 bar. Filled/empty circles represent adsorption/desorption. d) Comparison of C_2H_2 uptake for UTSA-200a and other best-performing materials at 0.01 bar. Neutron crystal structure of UTSA-200a·C_2D_2 at 200 K viewed along the f) *b* and e) *c* axis, determined from Rietveld analysis (the different nets are highlighted in purple and dark green for clarity). Color code: D, white; C (in C_2H_2) orange.

experimentally determined H-bonding length in UTSA-200a (1.921 Å) is notably shorter than that observed in SIFSIX-2-Cu-i (2.015 Å), further indicating that there are stronger interactions with C_2H_2 molecules. Consistent with this, the calculated static binding energy (ΔE) of C_2H_2 for UTSA-200a (56.0 kJ mol^{-1}) is larger than that of SIFSIX-2-Cu-i (52.9 kJ mol^{-1}), making it the strongest C_2H_2 adsorption observed in SIFSIX and related materials. This is the primary factor for the ultrahigh C_2H_2 adsorption capacity of UTSA-200a at very low pressures. Further diffraction measurement shows that the MOF structure can be completely restored after removing C_2D_2 from the sample, suggesting that the adsorption-induced lattice distortion is a temporary effect, and thus the sample does not lose crystallinity.

Given the observations of molecular exclusion of C_2H_4 and ultrastrong C_2H_2 capture capacity, UTSA-200a was found to exhibit an extraordinary ideal adsorbed solution theory (IAST) selectivity of over 6000 at 1 bar and 298 K for binary C_2H_2/C_2H_4 (1/99, v/v) mixtures, significantly higher than the previous top-performing materials (**Figure 3**a). It should be pointed out that this value is only for the qualitative comparison purpose. We also calculated the uptake ratios of C_2H_2/C_2H_4 (at 0.01/0.01 or 0.01/0.99 bar) determined from single-component isotherms[40] and compared with other reported MOFs (Figure S12, Supporting Information). These data also clearly demonstrate the superior selectivity of UTSA-200a for the separation of

C_2H_2/C_2H_4 mixtures. In addition, UTSA-200a also exhibits the highest C_2H_2 uptake (1.74 mol kg^{-1}) for adsorption from this gas mixture, which is much higher than the benchmark MOFs evaluated in Figure 3b. UTSA-200a is to our knowledge the first example of a porous material that fully overcomes the trade-off between selectivity and uptake capacity in which it exhibits not only the unprecedented high selectivity but also record-high uptake capacity in the context of C_2H_2/C_2H_4 separation.

Next, transient breakthrough simulations were performed to validate the feasibility of using UTSA-200a in a fixed bed for the separation of 1/99 C_2H_2/C_2H_4 mixture that mimics the industrial process. Figure 3c reveals the molar concentrations of C_2H_2/C_2H_4 exiting the adsorber packed with UTSA-200a as a function of the dimensionless time, τ, at 1 bar and 298 K. Complete separation was accomplished by UTSA-200a, whereby C_2H_4 breakthrough occurred first within seconds to yield the polymer-grade gas, and then C_2H_2 passed through the fixed bed after a certain time (τ_{break}). Attributed to the record-high selectivity and C_2H_2 uptake capacity, the τ_{break} value for UTSA-200a is more than twice as long as that observed in the previous benchmark, SIFSIX-2-Cu-i. Further, during the time $0-\tau_{break}$, the C_2H_2 amount captured by UTSA-200a reaches up to 2133.3 mmol L^{-1}, which is 3–30 times higher than SIFSIX-2-Cu-i (780.0 mmol L^{-1}) and other benchmark materials (Figure 3d). Overall, the separation performance of UTSA-200a far surpasses other SIFSIX materials and MOFs reported to date.
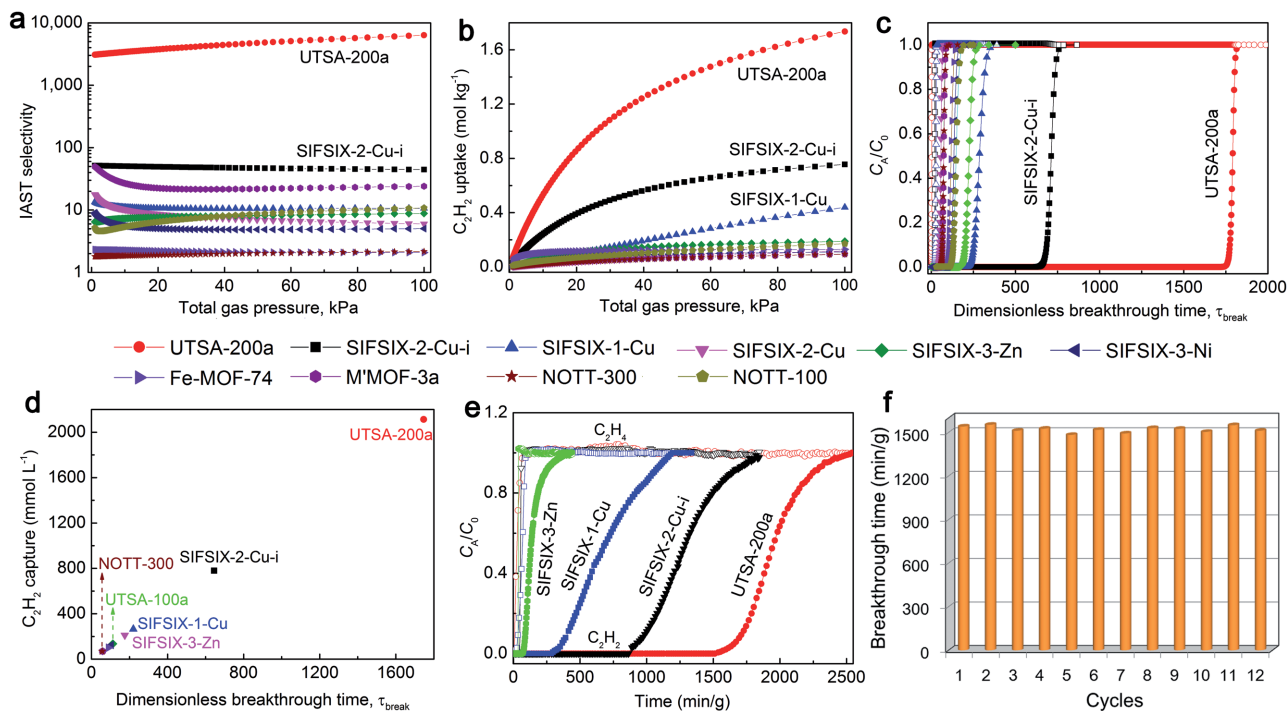
Figure 3. IAST calculations, simulated and experimental column breakthrough studies of UTSA-200a for C_2H_2/C_2H_4 (1/99) mixtures. Comparison of the a) IAST selectivity and b) C_2H_2 uptake capacity of UTSA-200a versus the other best-performing materials. c) Simulated column breakthrough curves for C_2H_2/C_2H_4 separation with respect to various MOF materials as indicated. d) Plots of the amount of C_2H_2 captured as a function of τ_{break} in the simulated column breakthrough for UTSA-200a and the other indicated materials. e) Experimental column breakthrough curves for C_2H_2/C_2H_4 separations with UTSA-200a, SIFSIX-2-Cu-i, SIFSIX-1-Cu, and SIFSIX-3-Zn at 298 K and 1.01 bar. f) The recyclability of UTSA-200a under multiple mixed-gas column breakthrough tests.

These simulated results prompted us to further evaluate the separation performance of UTSA-200a in the actual separation. Experimental breakthrough studies were conducted for a C_2H_2/C_2H_4 (1:99, v/v) mixture at room temperature. As illustrated in Figure 3e, highly efficient separation for C_2H_2/C_2H_4 mixture was achieved by UTSA-200a: the C_2H_4 gas eluted through the adsorption bed immediately in a high-purity grade (Figure S14, Supporting Information), whereas C_2H_2 was retained in the packed column over 1500 min (the concentration in the outlet below 40 ppm). This C_2H_2 breakthrough time is 2 times longer than SIFSIX-2-Cu-i (≈800 min), in good agreement with the simulated breakthrough results. Detailed gas chromatography data revealed that the purity of C_2H_2 in the outlet effluent was below 1 ppm up to 1300 min, affording high C_2H_4 purity of >99.9999% (Figure S15, Supporting Information). The C_2H_2 concentration is notably less than the acceptable level of <40 ppm for polymer-grade C_2H_4 gas. During the breakthrough process, the C_2H_4 production from the outlet effluent and the C_2H_2-captured amount for a given cycle were analyzed to be record high of 85.7 and 1.18 mmol g^{-1}, respectively, which is much higher than the 47.4 and 0.73 mmol g^{-1} observed in SIFSIX-2-Cu-i. The adsorbed C_2H_2 can be further recovered in a two-step process via adsorption followed by desorption at 338 K, offering a 93.6% recovery of a C_2H_2 capacity of 1.105 mmol g^{-1} per cycle, with a 97% purity (Figures S16 and S17, Supporting Information). This recovered C_2H_2 purity is notably higher than the 89% obtained in SIFSIX-2-Cu-i. These results indicate that

UTSA-200a offers the potential to effectively separate C_2H_2 from C_2H_4 and simultaneously produce both gases in high purity.

The feed gases in the practical C_2H_2 removal unit are often contaminated by trace levels of CO_2 (<50 ppm), H_2O (<5 ppm), and O_2 (<5 ppm),[43] so the amenability to recycling and efficacy in the presence of these gases must be also addressed. To investigate the influence of these other gases, we conducted a series of breakthrough experiments on UTSA-200a for the 1/99 mixtures containing trace amounts of CO_2, H_2O, and O_2, respectively. The presence of CO_2 (100 ppm) and O_2 (up to 2200 ppm) has a negligible effect on the separation capacity of UTSA-200a (Figures S18 and S19, Supporting Information). Similarly, the moisture (from 6 to 1340 ppm) also did not affect the separation of C_2H_2 from C_2H_4 (Figure S20, Supporting Information). Subsequently, we performed multiple mixed-gas (C_2H_2/C_2H_4 at 1/99) column breakthrough tests to examine the preservation of separation performance of UTSA-200a at ambient conditions. The recycling measurements revealed that UTSA-200a retains the C_2H_2 capture capacity and its molecular sieving over 12 cycles (Figures S21 and S23, Supporting Information). The breakthrough time remains almost unchanged during 12 breakthrough experiments, confirming the recyclability of this material for C_2H_2/C_2H_4 separation (Figure 3f). As inferred from the PXRD performed on associated samples, the framework of UTSA-200a remains stable after multiple adsorption and breakthrough experiments (Figure S27, Supporting Information).

Removal of acetylene from ethylene/acetylene mixture (1/99) is one of the most important but challenging industrial-scale gas separations and is currently affected by energy- and cost-intensive processes.[44–46] Although adsorption-based porous materials offer promise to create cost-effective and energy-efficient separation technologies, porous materials reported so far suffer from a trade-off between adsorption capacity and selectivity.[47–50] We have demonstrated the first example of nearly ideal molecular sieve, UTSA-200a, with the required characteristics (molecular-sieving size of ≈ 3.4 Å and strong binding sites toward C_2H_2), that afford the selective molecular exclusion of C_2H_4 and record-high amount of C_2H_2 adsorption, thus overcoming the trade-off effect for achieving highly efficient separation of C_2H_2/C_2H_4 mixtures. The molecular sieving of C_2H_2 from C_2H_4 is supported by detailed structural analysis, gas adsorption isotherms, simulated and experimental breakthrough studies. The resulting separation performance includes record-high C_2H_4 productivity of 87.5 mmol g^{-1} per cycle with purity higher than 99.9999% and simultaneous production of the high purity C_2H_2 (97%) via a simple recovery operation.

Ideal molecular sieves, while very difficult to achieve, indeed can provide a promising energy-efficient route to address the industrially important gas separations. Through fine tuning of pore size in molecular sieves to selectively exclude the C_2H_4 but to retain the strong binding sites for the record-high C_2H_2 adsorption capacity, our findings demonstrated, for the first time, that it is possible and feasible to target microporous MOFs with ideal molecular sieve performance through the elaborated fine tuning of the pore sizes and the introduction of specific binding sites for the preferred gas molecules. SIFSIX-14-Cu-i/UTSA-200 can readily remove trace amount of C_2H_2 from 1/99 C_2H_2/C_2H_4 mixture, affording benchmark high selectivity as well as benchmark C_2H_2 capture capacity and thus record-high C_2H_4 production scale as demonstrated in the breakthrough experiments. Combined with the excellent recyclability and resistance to other gases, SIFSIX-14-Cu-i/UTSA-200 represents an ideal microporous solid material that has the potential to be applied in the industry as an adsorbent for removing trace acetylene from ethylene using a relatively simple and energy-efficient process. The principle revealed in this work is general, which will provide some guidance to facilitate the design and implementation of ideal molecular sieves for other important gas separations and purification as well.

Supporting Information

Supporting Information is available from the Wiley Online Library or from the author.

Acknowledgements

Conflict of Interest

The authors declare no conflict of interest.

Keywords

[1] D. S. Sholl, R. P. Lively, *Nature* **2016**, *532*, 435.
[2] J. Y. S. Lin, *Science* **2016**, *353*, 121.
[3] S. Chu, Y. Cui, N. Liu, *Nat. Mater.* **2017**, *16*, 16.
[4] P. Taylor, *Energy Technology Perspectives 2010—Scenarios and Strategies to 2050*, International Energy Agency, Paris **2010**, p. 74.
[5] S. M. Kuznicki, V. A. Bell, S. Nair, H. W. Hillhouse, R. M. Jacubinas, C. M. Braunbarth, B. H. Toby, M. Tsapatsis, *Nature* **2001**, *412*, 720.
[6] S. Kucnicki, V. Bell, *US6517611*, **2003**.
[7] R. T. Yang, *Adsorbents: fundamentals and applications*, Wiley, Hoboken, NJ **2003**.
[8] H. Furukawa, K. E. Cordova, M. O'Keeffe, O. M. Yaghi, *Science* **2013**, *341*, 974.
[9] H. Sato, W. Kosaka, R. Matsuda, A. Hori, Y. Hijikata, R. V. Belosludov, S. Sakaki, M. Takata, S. Kitagawa, *Science* **2014**, *343*, 167.
[10] G. Férey, C. Serre, *Chem. Soc. Rev.* **2009**, *38*, 1380.
[11] Z. R. Herm, B. M. Wiers, J. A. Mason, J. M. van Baten, M. R. Hudson, P. Zajdel, C. M. Brown, N. Masciocchi, R. Krishna, J. R. Long, *Science* **2013**, *340*, 960.
[12] J. R. Li, J. Sculley, H. C. Zhou, *Chem. Rev.* **2012**, *112*, 869.
[13] O. K. Farha, I. Eryazici, N. C. Jeong, B. G. Hauser, C. E. Wilmer, A. A. Sarjeant, R. Q. Snurr, S. T. Nguyen, A. Ö. Yazaydın, J. T. Hupp, *J. Am. Chem. Soc.* **2012**, *134*, 15016.
[14] S. Yang, X. Lin, A. J. Blake, G. S. Walker, P. Hubberstey, N. R. Champness, M. Schröder, *Nat. Chem.* **2009**, *1*, 487.
[15] J. W. Yoon, Y.-K. Seo, Y. K. Hwang, J.-S. Chang, H. Leclerc, S. Wuttke, P. Bazin, A. Vimont, M. Daturi, E. Bloch, P. L. Llewellyn, C. Serre, P. Horcajada, J.-M. Grenèche, A. E. Rodrigues, G. Férey, *Angew. Chem., Int. Ed.* **2010**, *49*, 5949.
[16] S. Krause, V. Bon, I. Senkovska, U. Stoeck, D. Wallacher, D. M. Többens, S. Zander, R. S. Pillai, G. Maurin, F.-X. Coudert, S. Kaskel, *Nature* **2016**, *532*, 348.
[17] K. Adil, Y. Belmabkhout, R. S. Pillai, A. Cadiau, P. M. Bhatt, A. H. Assen, G. Maurin, M. Eddaoudi, *Chem. Soc. Rev.* **2017**, *46*, 3402.
[18] P. Nugent, Y. Belmabkhout, S. D. Burd, A. J. Cairns, R. Luebke, K. Forrest, T. Pham, S. Ma, B. Space, L. Wojtas, M. Eddaoudi, M. J. Zaworotko, *Nature* **2013**, *495*, 80.
[19] K. Li, D. H. Olson, J. Seidel, T. J. Emge, H. Gong, H. Zeng, J. Li, *J. Am. Chem. Soc.* **2009**, *131*, 10368.
[20] R. K. Motkuri, H. V. R. Annapureddy, M. Vijaykumar, H. T. Schaef, P. F. Martin, B. P. McGrail, L. X. Dang, R. Krishna, P. K. Thallapally, *Nat. Commun.* **2014**, *5*, 4368.
[21] P.-Q. Liao, W.-X. Zhang, J.-P. Zhang, X.-M. Chen, *Nat. Commun.* **2015**, *6*, 8697.
[22] Q.-G. Zhai, X. Bu, C. Mao, X. Zhao, L. Daemen, Y. Cheng, A. J. Ramirez-Cuesta, P. Feng, *Nat. Commun.* **2016**, *7*, 13645.
[23] R. Vaidhyanathan, S. S. Iremonger, G. K. H. Shimizu, P. G. Boyd, S. Alavi, T. K. Woo, *Science* **2010**, *330*, 650.

[24] B. Li, Y. Zhang, R. Krishna, K. Yao, Y. Han, Z. Wu, D. Ma, Z. Shi, T. Pham, B. Space, J. Liu, P. K. Thallapally, J. Liu, M. Chrzanowski, S. Ma, *J. Am. Chem. Soc.* **2014**, *136*, 8654.

[25] N. T. T. Nguyen, H. Furukawa, F. Gándara, H. T. Nguyen, K. E. Cordova, O. M. Yaghi, *Angew. Chem., Int. Ed.* **2014**, *53*, 10645.

[26] J. W. Yoon, H. Chang, S.-J. Lee, Y. K. Hwang, D.-Y. Hong, S.-K. Lee, J. S. Lee, S. Jiang, T.-U. Yoon, K. Kwac, Y. Jung, R. S. Pillai, F. Faucher, A. Vimont, M. Daturi, G. Férey, C. Serre, G. Maurin, Y.-S. Bae, J.-S. Chang, *Nat. Mater.* **2017**, *16*, 526.

[27] Y.-S. Bae, C. Y. Lee, K. C. Kim, O. K. Farha, P. Nickias, J. T. Hupp, S. T. Nguyen, R. Q. Snurr, *Angew. Chem., Int. Ed.* **2012**, *51*, 1857.

[28] X. Cui, K. Chen, H. Xing, Q. Yang, R. Krishna, Z. Bao, H. Wu, W. Zhou, X. Dong, Y. Han, B. Li, Q. Ren, M. J. Zaworotko, B. Chen, *Science* **2016**, *353*, 141.

[29] A. Cadiau, K. Adil, P. M. Bhatt, Y. Belmabkhout, M. Eddaoudi, *Science* **2016**, *353*, 137.

[30] R. T. Yang, *Gas Separation by Adsorption Processes*, Butterworth Publishers, Boston, **1986**.

[31] C. A. Grande, A. E. Rodrigues, *Ind. Eng. Chem. Res.* **2005**, *44*, 8815.

[32] D.-Y. Koh, B. A. McCool, H. W. Deckman, R. P. Lively, *Science* **2016**, *353*, 804.

[33] C. A. Grande, V. M. T. M. Silva, C. Gigola, A. E. Rodrigues, *Carbon* **2003**, *41*, 2533.

[34] J. M. S. Denny, J. C. Moreton, L. Benz, S. M. Cohen, *Nat. Rev. Mater.* **2016**, *1*, 16078.

[35] M. Carta, R. Malpass-Evans, M. Croad, Y. Rogan, J. C. Jansen, P. Bernardo, F. Bazzarelli, N. B. McKeown, *Science* **2013**, *339*, 303.

[36] A. Ghoufi, K. Benhamed, L. Boukli-Hacene, G. Maurin, *ACS Cent. Sci.* **2017**, *3*, 394.

[37] L. Hamon, P. L. Llewellyn, T. Devic, A. Ghoufi, G. Clet, V. Guillerm, G. D. Pirngruber, G. Maurin, C. Serre, G. Driver, W. V. Beek,

E. Jolimaître, A. Vimont, M. Daturi, G. Férey, *J. Am. Chem. Soc.* **2009**, *131*, 17490.

[38] P. M. Bhatt, Y. Belmabkhout, A. Cadiau, K. Adil, O. Shekhah, A. Shkurenko, L. J. Barbour, M. Eddaoudi, *J. Am. Chem. Soc.* **2016**, *138*, 9301.

[39] O. Shekhah, Y. Belmabkhout, Z. Chen, V. Guillerm, A. Cairns, K. Adil, M. Eddaoudi, *Nat. Commun.* **2014**, *5*, 4228.

[40] K.-J. Chen, D. G. Madden, T. Pham, K. A. Forrest, A. Kumar, Q.-Y. Yang, W. Xue, B. Space, J. J. PerryIV, J.-P. Zhang, X.-M. Chen, M. J. Zaworotko, *Angew. Chem., Int. Ed.* **2016**, *55*, 10268.

[41] A. H. Assen, Y. Belmabkhout, K. Adil, P. M. Bhatt, D.-X. Xue, H. Jiang, M. Eddaoudi, *Angew. Chem., Int. Ed.* **2015**, *54*, 14353.

[42] J.-R. Li, R. J. Kuppler, H.-C. Zhou, *Chem. Soc. Rev.* **2009**, *38*, 1477.

[43] K. M. Sundaram, M. M. Shreehan, E. F. Olszewski, "Ethylene," in *Firk-Othmer Encyclopedia of Chemical Technology*, Wiley Online Library, New York, **2001**.

[44] F. Studt, F. Abild-Pedersen, T. Bligaard, R. Z. Sørensen, C. H. Christensen, J. K. Nørskov, *Science* **2008**, *320*, 1320.

[45] J. D. Lewis, *US 3,837,144*, **1974**.

[46] R. Matsuda, R. Kitaura, S. Kitagawa, Y. Kubota, R. V. Belosludov, T. C. Kobayashi, H. Sakamoto, T. Chiba, M. Takata, Y. Kawazoe, Y. Mita, *Nature* **2005**, *436*, 238.

[47] E. D. Bloch, W. L. Queen, R. Krishna, J. M. Zadrozny, C. M. Brown, J. R. Long, *Science* **2012**, *335*, 1606.

[48] Z. Bao, G. Chang, H. Xing, R. Krishna, Q. Ren, B. Chen, *Energy Environ. Sci.* **2016**, *9*, 3612.

[49] T.-L. Hu, H. Wang, B. Li, R. Krishna, H. Wu, W. Zhou, Y. Zhao, Y. Han, X. Wang, W. Zhu, Z. Yao, S. Xiang, B. Chen, *Nat. Commun.* **2015**, *6*, 7328.

[50] S. Yang, A. J. Ramirez-Cuesta, R. Newby, V. Garcia-Sakai, P. Manuel, S. K. Callear, S. I. Campbell, C. C. Tang, M. Schröder, *Nat. Chem.* **2014**, *7*, 121.

ADVANCED MATERIALS

Supporting Information

An Ideal Molecular Sieve for Acetylene Removal from Ethylene with Record Selectivity and Productivity

Bin Li, Xili Cui, Daniel O'Nolan, Hui-Min Wen, Mengdie Jiang, Rajamani Krishna, Hui Wu, Rui-Biao Lin, Yu-Sheng Chen, Daqiang Yuan, Huabin Xing,* Wei Zhou,* Qilong Ren, Guodong Qian, Michael J. Zaworotko,* and Banglin Chen*

Supplementary Information

An Ideal Molecular Sieve for Acetylene Removal from Ethylene with Record Selectivity and Productivity

Bin Li[†], Xili Cui[†], Dan O'Nolan[†], Hui-Min Wen, Mengdie Jiang, Rajamani Krishna, Hui Wu, Rui-Biao Lin, Yu-Sheng Chen, Daqiang Yuan, Huabin Xing*, Wei Zhou*, Qilong Ren, Guodong Qian, Michael J. Zaworotko*, and Banglin Chen*

Dr. B. Li,[†] Prof. G. Qian, Prof. B. Chen
State Key Laboratory of Silicon Materials, Cyrus Tang Center for Sensor Materials and Applications, School of Materials Science and Engineering, Zhejiang University, Hangzhou, 310027, China
E-mail: banglin.chen@utsa.edu
Dr. H.-M. Wen, Dr. R.-B. Lin, Prof. B. Chen
Department of Chemistry, University of Texas at San Antonio, One UTSA Circle, San Antonio, Texas 78249-0698, USA
Dr. X. Cui, [†] M. Jiang, Prof. H. Xing, Prof. Q. Ren
Key Laboratory of Biomass Chemical Engineering of Ministry of Education, College of Chemical and Biological Engineering, Zhejiang University, Hangzhou 310027, China
E-mail: xinghb@zju.edu.cn
D. O'Nolan, [†] Prof. M. J. Zaworotko
Department of Chemical and Environmental Sciences, University of Limerick, Limerick, Republic of Ireland
E-mail: michael.zaworotko@ul.ie
Prof. R. Krishna
Van't Hoff Institute for Molecular Sciences, University of Amsterdam, Science Park 904, 1098 XH Amsterdam, Netherlands
Dr. H. Wu, Dr. W. Zhou
NIST Center for Neutron Research, National Institute of Standards and Technology, Gaithersburg, MD 20899-6102, USA
E-mail: wzhou@nist.gov
Dr. Y.-S. Chen
ChemMatCARS, Center for Advanced Radiation Sources, The University of Chicago, 9700 South Cass Avenue, Argonne, Illinois 60439, USA
Prof. D. Yuan
State Key Laboratory of Structure Chemistry, Fujian Institute of Research on the Structure of Matter, Chinese Academy of Sciences, Fuzhou, Fujian 350002, China
[†]These authors contributed equally to this work.

1. General Materials and MOF Synthesis

All starting chemicals and solvents were purchased from commercial companies and used without further purification. Thermogravimetric analyses (TGA) were carried out using a Shimadzu TGA-50 analyzer under N_2 atmosphere with a heating rate of 5 $^{\circ}$C min^{-1}. Powder X–ray diffraction (PXRD) patterns were measured by a Rigaku Ultima IV diffractometer operated at 40 kV and 44 mA with a scan rate of 2.0 deg min^{-1}.

N_2 (99.999%), C_2H_2 (99%), C_2H_4 (99.99%), He (99.999%) and mixed gases of (1) C_2H_2/C_2H_4 = 1/99 (v/v), (2) 100 ppm CO_2, 1% C_2H_2 and 98.99% C_2H_4; (3) 1000 ppm CO_2, 1% C_2H_2 and 98.9% C_2H_4 were purchased from JinGong Company (China). Mixed gases of (4) 6 ppm H_2O, 1% C_2H_2 and 98.99% C_2H_4, (5) 83 ppm H_2O, 1% C_2H_2 and 98.99% C_2H_4, (6) 1340 ppm H_2O, 1% C_2H_2, and 98.86% C_2H_4, and standard gases of C_2H_2 and C_2H_4 were purchased from Shanghai Wetry Standard Reference Gas Analytical Technology Co. LTD (China).

Synthesis of [Cu(azpy)$_2$(SiF$_6$)]$_n$ (SIFSIX-14-Cu-i/UTSA-200). Saffron prism-shaped single crystals of SIFSIX-14-Cu-i/UTSA-200 were synthesized in quantitative yield at room temperature by slow diffusion of a methanol solution of CuSiF$_6$ (2 mL, 0.15 mmol) into a DMSO solution of 4,4 -azopyridine (azpy, 0.12 mmol) after one week. An alternative fast and direct mixing method was used to produce large amount of powder samples of SIFSIX-14-Cu-i/UTSA-200. A methanol solution (3 mL) of azpy (0.266 mmol) was mixed with an aqueous solution of CuSiF$_6$ (2.5 mL, 0.247 mmol) at 80°C resulting in a bright grey precipitate, which was then heated at 80°C for 15 min, additional 1 h at 50°C, and then at room temperature for 24 h (86% yield based on azpy).

2. Gas sorption measurements

A Micromeritics ASAP 2020 surface area analyzer was used to measure gas adsorption isotherms. To remove all the guest solvents in the framework, the fresh powder samples were first solvent-exchanged with dry methanol at least 10 times within two days, and evacuated at room temperature (298 K) for 36 h until the outgas rate was 5 mmHg min^{-1} prior to measurements. The sorption measurement was maintained at 77 K or 196 K under liquid nitrogen or dry ice-acetone bath, respectively. An ice-water bath (slush) and water bath were used for adsorption isotherms at 273 and 298 K, respectively.

3. Breakthrough tests

   The breakthrough experiments were performed in dynamic gas breakthrough equipment similarly to our previous work.[1] All experiments were conducted using a stainless steel column (4.6 mm inner diameter × 50 mm). The weight of sample packed in the column was: 0.158 g. The column packed with sample was firstly purged with He flow (10 ml min⁻¹) for 12 h at room temperature (25 °C). The mixed gas (C_2H_2/C_2H_4: 1/99, v/v) flow was then introduced at 1.25 ml min⁻¹. Outlet gas from the column was monitored using gas chromatography (GC-8A or GC-2010 plus, SHIMADZU) with a flame ionization detector (FID). The standard gases were used to calibrate the concentration of the outlet gas. After the breakthrough experiment, the sample was regenerated with He flow (7 to 14 ml min⁻¹) for 6 to 20 hours.

   The captured C_2H_2 by UTSA-200a during the breakthrough experiment can be recovered in a two-step process by adsorption followed by desorption at 338 K. Detection of the composition of gases during regeneration process is shown as follows: to analysis the composition of the desorbed gases, we firstly introduced the mixed gas (71.775% C_2H_4, 27.5 N_2, 0.725% C_2H_2) into the column (UTSA-200a) at 1.91 ml/min. When the breakthrough experiments were finished, heated the column to 338 K with the unchanged flow rate of 71.775% C_2H_4, 27.5 N_2, 0.725% C_2H_2. Outlet gas from the column was monitored using gas chromatography (GC-2010 plus) with a thermal conductivity detector (TCD) coupled with a FID. It should be note that nitrogen in the mixed gas was used to calibrate the change of flow rate during desorption process. By subtracting the background signal from the collected data, we got the composition of the desorbed C_2H_2 and C_2H_4.

   In the processes of production of high-purity C_2H_4, the feed gases for the unit of C_2H_2 removal are contaminated with trace levels of CO_2 (< 50 ppm), H_2O (< 5 ppm), and O_2 (< 5 ppm).[2] Therefore, the effect of trace levels of CO_2 (< 100 ppm), H_2O (< 1340 ppm), and O_2 (< 2200 ppm) on the separation of C_2H_2/C_2H_4 mixtures was also investigated. Breakthrough tests of mixed gas ($C_2H_2/C_2H_4/CO_2$ or $C_2H_2/C_2H_4/O_2$): The mixed gas flow was introduced at 1.25 ml min⁻¹. Outlet gas from the column was monitored using gas chromatography (GC-2010 plus) with a thermal conductivity detector (TCD) coupled with a FID. The gas mixture was separated by a capillary column (Agilent GS-GASPRO, 0.32 × 60 M) at 373 K with a He flow rate of 8 mL/min. The

concentration of CO_2 or O_2 in the outlet gas was monitored by a TCD and the concentration of C_2H_2 and C_2H_4 were detected by a FID. Breakthrough tests of mixed gas ($C_2H_2/C_2H_4/H_2O$): the mixed gas flow was introduced at 1.25 ml min^{-1}. Outlet gas from the column was monitored using two gas chromatography in a series. The first gas chromatography is a GC-2010 plus with a TCD and a capillary column (Agilent HP-PLOT/Q, 0.53 × 30 M). The second gas chromatography is a GC-8A with a FID and a packed column (No. 15092203, JieDao Tech). The concentration of H_2O in the outlet gas was monitored by a TCD (GC-2010 plus) and the concentration of C_2H_2 and C_2H_4 were detected by a FID (GC-8A).

4. Single-crystal X-ray crystallography

Crystal data of UTSA-200 were collected using synchrotron radiation, = 0.41325 , at the Advanced Photon Source, Chicago, IL. Indexing was performed using APEX2 (Difference Vectors method).[3] Data integration and reduction were performed using SaintPlus 6.0.[4] Absorption correction was performed by multi-scan method implemented in SADABS.[5] Space groups were determined using XPREP implemented in APEX2.[3] The structure was solved by direct methods and refined by full matrix least-squares methods with the SHELX-97 program package.[6,7] The solvent molecules in the compound are highly disordered. The SQUEEZE subroutine of the PLATON software suite was used to remove the scattering from the highly disordered guest molecules.[8] The resulting new files were used to further refine the structures. The H atoms on C atoms were generated geometrically. The crystal data are summarized in Table S2.

5. Neutron diffraction experiment

Neutron diffraction data were collected using the BT-1 neutron powder diffractometer at the National Institute of Standards and Technology (NIST) Center for Neutron Research. A Ge(311) monochromator with a 75° take-off angle, λ = 2.0787(2) Å, and in-pile collimation of 60 minutes of arc was used. Data were collected over the range of 1.3-166.3° (2θ) with a step size of 0.05°. Fully activated UTSA-200a sample was loaded in a vanadium can equipped with a capillary gas line and a packless valve. A closed-cycle He refrigerator was used for sample temperature control. The bare MOF sample was measured first at the temperatures of 6 K, 100 K, 200 K, and 300 K. To probe the acetylene adsorption locations, a pre-determined amount of C_2D_2 (~1.64 C_2D_2 per UTSA-200a; note that deuterated acetylene was used because H has large incoherent

neutron scattering cross section, and thus would introduce large background in the diffraction data) was loaded into the sample at room temperature, and the sample was slowly cooled to 200 K (at which point, nearly all gas molecules were adsorbed into the sample). Diffraction data were then collected on the C_2D_2-loaded MOF samples.

Rietveld structural refinement was performed on the neutron diffraction data using the GSAS package.[9] Refinement on lattice parameters, atomic coordinates, thermal factors, gas molecule occupancies, background, and profiles all converge with satisfactory R-factors. The structural data are summarized in Table S3 and S4.

6. Density-functional theory calculations

Neutro First-principles density-functional theory (DFT) calculations were performed using the Quantum-Espresso package. A semi-empirical addition of dispersive forces to conventional DFT was included in the calculation to account for van der Waals interactions.[10] We used Vanderbilt-type ultrasoft pseudopotentials and generalized gradient approximation (GGA) with Perdew-Burke-Ernzerhof (PBE) exchange correlation. A cutoff energy of 544 Ev and a 2×2×4 k-point mesh (generated using the Monkhosrt-Pack scheme) were found to be enough for the total energy to converge within 0.01 meV/atom. We first optimized the structure of UTSA-200a. The optimized structures are good matches for the experimentally determined crystal structures of the coordination networks. Various guest gas molecules were then introduced to various locations of the channel pore, followed by a full structural relaxation. To obtain the gas binding energy, an isolated gas molecule placed in a supercell (with the same cell dimensions as the MOF crystal) was also relaxed as a reference. The static binding energy (at T = 0 K) was then calculated using:
EB = E(MOF) + E(gas) – E(MOF+gas).

7. Fitting of pure component isotherms

The pure component isotherm data for C_2H_2 and C_2H_4 in UTSA-200 were fitted with the dual-site Langmuir-Freundlich isotherm model

$$q = q_{A,sat} \frac{b_A p^{vA}}{1 + b_A p^{vA}} + q_{B,sat} \frac{b_B p^{vB}}{1 + b_B p^{vB}} \tag{1}$$

with T-dependent parameters b_A, and b_B

$$b_A = b_{A0} \exp\left(\frac{E_A}{RT}\right); \quad b_B = b_{B0} \exp\left(\frac{E_B}{RT}\right) \tag{2}$$

The fitted parameter values are presented in Table S6. For all other MOFs, the isotherm data are taken from Cui et al. and Hu et al.[1,11]

8. Isosteric heat of adsorption

The binding energy of C_2H_2 is reflected in the isosteric heat of adsorption, Q_{st}, defined as

$$Q_{st} = RT^2 \left(\frac{\partial \ln p}{\partial T}\right)_q \tag{3}$$

Fig. S10 presents a comparison of the heats of adsorption of C_2H_2 for UTSA-200a with SIFSIX-2-Cu-i; the calculations are based on the use of the Clausius-Clapeyron equation.

9. IAST calculations of adsorption selectivities

We consider the separation of binary C_2H_2/C_2H_4 mixtures. The adsorption selectivity for C_2H_2/C_2H_4 separation is defined by

$$S_{ads} = \frac{q_1/q_2}{p_1/p_2} \tag{4}$$

In equation (4), q_1 and q_2 are the molar loadings in the adsorbed phase in equilibrium with the bulk gas phase with partial pressures p_1, and p_2. Fig. 3a presents IAST calculations of the adsorption selectivity and uptake capacity of C_2H_2/C_2H_4 mixtures containing 1% C_2H_2, as a function of the total bulk gas pressure.

10. Transient breakthrough of C_2H_2/C_2H_4 mixtures in fixed bed adsorbers

The performance of industrial fixed bed adsorbers is dictated by a combination of adsorption selectivity and uptake capacity. For a proper comparison of various MOFs, we perform transient breakthrough simulations using the simulation methodology described in the literature.[12,13] For the breakthrough simulations, the following parameter values were used: length of packed bed, L = 0.12 m; voidage of packed bed, = 0.75; superficial gas velocity at inlet, u = 0.003 m/s. The transient breakthrough simulation results are presented in terms of a dimensionless time, , defined by dividing the actual time, t, by the characteristic time, $\frac{L\varepsilon}{u}$.

We investigated the separation performance of UTSA-200a for the separation of 1/99 C_2H_2/C_2H_4 feed mixtures. The transient breakthrough simulations in Fig. 3c show the molar concentrations of C_2H_2/C_2H_4 in the gas phase exiting the adsorber packed with UTSA-200a as a function of the dimensionless time, . In these simulations, the total bulk gas phase is at 298 K and 100 kPa; the partial pressures of C_2H_2, and C_2H_4 in the inlet feed gas mixture are, respectively, p_1 = 1 kPa, p_2 = 99 kPa. Analogous breakthrough simulations were performed for UTSA-200a. On the basis of the gas phase concentrations, we can calculate the impurity level of C_2H_2 in the gas mixture exiting the fixed bed packed with UTSA-200a; see Fig. S13. At a certain time, $_{break}$, the impurity level will exceed the desired purity level of 40 ppm that corresponds to the purity requirement of the feed to the polymerization reactor. The adsorption cycle needs to be terminated at that time break and the regeneration process needs to be initiated. From a material balance on the adsorber, the amount of C_2H_2 captured during the time interval 0 - $_{break}$ can be determined. Table S7 provides a summary of the breakthrough times, $_{break}$ for various MOFs and the amount of C_2H_2 captured, expressed in mmol per L adsorbent in fixed bed. Fig. 3d presents a plot of the amount of C_2H_2 captured plotted as a function of the time interval $_{break}$. The hierarchy of capture capacities is directly related to the corresponding hierarchy of breakthrough times, $_{break}$. UTSA-200 has a significantly higher capture capacity, by more than a factor two, than other MOFs.

11. The studies of recyclability and the effect of moisture

The recyclability studies on C_2H_2 adsorption and breakthrough experiments were evaluated in UTSA-200a. The C_2H_2 adsorption isotherms were tested over 20 cycles on UTSA-200a. As shown in Fig. S24, the C_2H_2 uptake capacity shows no apparent loss after the cycling test. Similarly, we performed multiple mixed-gas (C_2H_2/C_2H_4 at 1/99) column breakthrough tests to examine the preservation of separation performance of UTSA-200a at ambient conditions. The recycling measurements revealed that UTSA-200a retains the C_2H_2 capture capacity and breakthrough time over at least 12 cycles (Fig. S21 and S23).

The effect of moisture on breakthrough experiments was carried out on UTSA-200a for the 1/99 C_2H_2/C_2H_4 mixtures containing trace H_2O (from 6 to 1340 ppm). The presence of trace H_2O has a negligible effect on the breakthrough performance of UTSA-200a (Fig. S20). When exposed the sample to a high humidity for a long time, UTSA-200 shows a very slow phase change, as indicated by PXRD peak shifts and the appearance of additional peaks. It is worth

noting that the changed sample can be regenerated to the original material by soaking into the methanol solution for 1 day, as confirmed by PXRD analyses (Fig. S25). Gas sorption measurements indicated that the regenerated sample remains the molecular sieving effect for C_2H_2/C_2H_4 separation without loss of the C_2H_2 adsorption capacity over three regeneration cycles (Fig. S26).

Table S1. Comparison of the adsorption uptakes, selectivities, and heat of adsorption data for C_2H_2 and C_2H_4 in UTSA-200a with some other reported MOFs.

MOFs	$S_{BET}{}^a$ (m²/g)	Pore size (Å)	Adsorption uptake[b]		Selectivity[c]	Q_{st} (KJ/mol)[d]		ΔE (KJ/mol)		Ref.
			C_2H_2 (mmol/g)	C_2H_4 (mmol/g)		C_2H_2	C_2H_4	C_2H_2	C_2H_4	
UTSA-200a	612^e	3.4×3.4	3.65	0.63	6320^f	40	$27/37^g$	56.0	–	This work
SIFSIX-2-Cu-i	503	4.4×4.4	4.02	2.19	44.54	41.9	30.7	52.9	39.8	1
M'MOF-3a	110	3.4×3.8	1.9^g	0.4^h	24	25	–	–	–	14
UTSA-100a	970	4.3×4.3	4.27^g	1.66^g	10.72	22	–	–	–	11
SIFSIX-1-Cu	1178	8.0×8.0	8.50	4.11	10.63	$30/37^g$	23.5	44.6	27.2	1
SIFSIX-3-Zn	250	4.2×4.2	3.64	2.24	8.82	$21/31^g$	28.8	50.3	47.4	1
SIFSIX-2-Cu	1881	11×11	5.38	2.02	6.0	26.3	20.8	34.6	–	1
SIFSIX-3-Ni	368	4.2×4.2	3.30	1.75	5.03	30.5	20.3	–	–	1
NOTT-300	1370	6.5×6.5	6.34^i	4.28^i	2.17	32	–	–	–	15
Fe-MOF-74	1350	11×11	6.8^j	6.1^j	2.08	46	–	–	–	16

[a] BET surface area calculated from N_2 isotherms at 77 K.

[b] At a temperature of 298 K.

[c] IAST selectivity for C_2H_2/C_2H_4 mixtures containing 1% C_2H_2 at 1 bar.

[d] Q_{st} values at low surface coverage.

[e] BET surface area calculated from CO_2 isotherms at 196 K.

[f] Only for the qualitative comparison.

[g] The highest Q_{st} values at various surface coverage.

[h] At a temperature of 296 K.

[i] At a temperature of 293 K.

[j] At a temperature of 318 K.

Table S2. Crystallographic data and structure refinement results of UTSA-200.

	UTSA-200
Formula	$C_{20}H_{16}CuF_6N_8Si$
Formula weight	574.04
Temperature/K	150(2)
Crystal system	Tetragonal
Space group	I-4
a, b (Å)	13.0634(12)
c (Å)	8.1827(7)
α (°)	90.00
β (°)	90.00
γ (°)	90.00
V (Å^3)	1396.4(3)
Z	2
D_{calcd} (g cm^{-3})	1.365
μ (mm^{-1})	0.211
$F(000)$	578.0
Crystal size/mm^3	$0.008 \times 0.006 \times 0.005$
GOF	1.108
R_{int}	0.1181
R_1, wR_2 [I>=2σ (I)]	0.0744, 0.1943
R_1, wR_2 [all data]	0.0802, 0.2079
Largest diff. peak and hole	0.714 and -0.870 e/Å^{-3}
CCDC number	1540995

Table S3. Structural data of the desolvated UTSA-200a.

Unit cell parameters of UTSA-200	
Formula	$C_{20}H_{16}CuF_6N_8Si$
Formula weight	574.04
Temperature/K	200(2)
Crystal system	Tetragonal
Space group	P4/nnc
a, b (Å)	13.0468(11)
c (Å)	7.9013(7)
α (°)	90.00
β (°)	90.00
γ (°)	90.00
V (Å^3)	1344.95(30)
Z	2
D_{calcd} (g cm^{-3})	1.4175
R_{wp}, R_p	0.0260, 0.0206
CCDC number	1541108

Table S4. The C_2D_2-loaded structural data for UTSA-200a· $1.64C_2D_2$.

Unit cell parameters of UTSA-200· $1.64C_2D_2$	
Formula	$C_{23.28}H_{16}CuD_{3.28}F_6N_{8.00}$ Si
Formula weight	619.98
Temperature/K	200(2)
Crystal system	Triclinic
Space group	P-1
a (Å)	13.0777(23)
b (Å)	13.0935(22)
c (Å)	8.1177(13)
α (°)	87.240(13)
β (°)	89.680(14)
γ (°)	89.866(31)
V (Å^3)	1388.4(5)
Z	2
R_{wp}, R_p	0.0312, 0.0247
CCDC number	1540994

Table S5. Comparison of C_2H_2 and C_2H_4 uptake (cm^3/cm^3) from gas sorption isotherms at various pressures, and the C_2H_2/C_2H_4 uptake ratio at 0.01/0.01 bar and 0.01/0.99 bar for various MOF materials indicated in this study.

MOFs	C_2H_2 uptake [$cm^3\,cm^{-3}$][a]	C_2H_4 uptake [$cm^3\,cm^{-3}$]			C_2H_2/C_2H_4 uptake ratio		Framework Density [$g\,cm^{-3}$]	Ref.
		0.01 bar	0.5 bar	0.99 bar	0.01/0.01[b]	0.01/0.99[c]		
UTSA-200a	57.8	0.062	4.5	18.4	929	3.41	1.417	This work
SIFSIX-2-Cu-i	42.1	1.7	44.4	61.0	25.2	0.70	1.247	1
M'MOF-3	6.5	0.5	9.3	13.7	13.0	0.51	1.040	17
SIFSIX-1-Cu	19.8	1.7	47.4	76.0	11.8	0.26	0.864	1
SIFSIX-3-Zn	17.8	1.6	69.8	75.7	11.1	0.23	1.578	1
UTSA-100a	18.1	5.7	36.4	42.4	3.2	0.43	1.062	11
Fe-MOF-74	31.7	22.7	129.6	151.6	1.4	0.20	1.126	16
NOTT-300	6.4	4.2	76.5	99.8	1.5	0.06	1.146	15
Mg-MOF-74	50.4	34.4	127.1	142.1	1.5	0.35	0.909	14

[a] The C_2H_2 uptake capacity at 0.01 bar and room temperature.

[b] The ratio from C_2H_2 uptake at 0.01 bar/C_2H_4 uptake at 0.01 bar (0.01/0.01).

[c] The ratio from C_2H_2 uptake at 0.01 bar/C_2H_4 uptake at 0.99 bar (0.01/0.99).

Table S6. Dual-site Langmuir-Freundlich parameter fits for C_2H_2 and C_2H_4 in UTSA-200.

	Site A				Site B			
	$q_{A,sat}$	b_{A0}	v_A	E_A	$q_{B,sat}$	b_{B0}	v_A	E_B
	mol kg^{-1}	Pa^{-vA}		kJ mol^{-1}	mol kg^{-1}	Pa^{-vB}		kJ mol^{-1}
C_2H_2	2.1	2.85×10^{-9}	1	22	2.3	2.93×10^{-10}	1	40
C_2H_4	1.3	1.36×10^{-53}	4.4	173	1.3	6.21×10^{-11}	1	25.4

Table S7. Breakthrough calculations for separation of C_2H_2/C_2H_4 mixture containing 1 mol% C_2H_2 at 298 K. The data for FeMOF-74 is at a temperature of 318 K; this is the lowest temperature used in the isotherm measurements of Bloch et al.[16] The data for NOTT-300 is at 293 K, for which the isotherm data is available in Yang et al.[15] The product gas stream contains less than 40 ppm C_2H_2.

MOFs	Dimensionless breakthrough time τ_{break}	C_2H_2 adsorbed during 0-τ_{break} mmol L^{-1}
UTSA-200	1746.1	2113.3
SIFSIX-2-Cu-i	644.90	780.00
SIFSIX-1-Cu	219.83	265.33
SIFSIX-3-Zn	175.16	211.00
UTSA-100a	112.39	135.33
SIFSIX-3-Ni	103.73	124.67
FeMOF-74	89.40	100.67
M'MOF-3a	58.45	69.67
NOTT-300	56.28	68.33
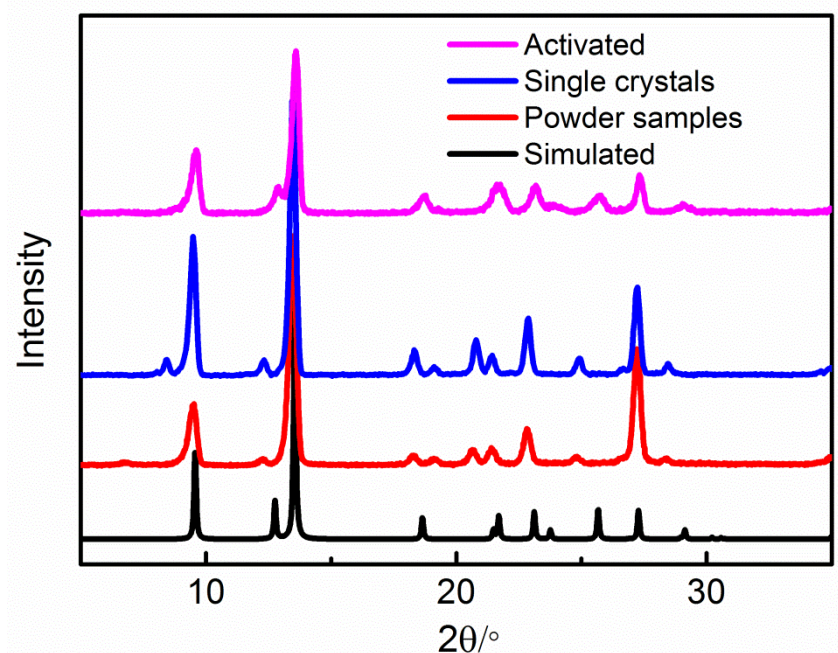
Figure S1. PXRD patterns of as-synthesized powder (red) and single-crystal samples (blue) of UTSA-200 (red), and activated UTSA-200a (pink) along with the simulated XRD pattern from the single-crystal X-ray structure (black).
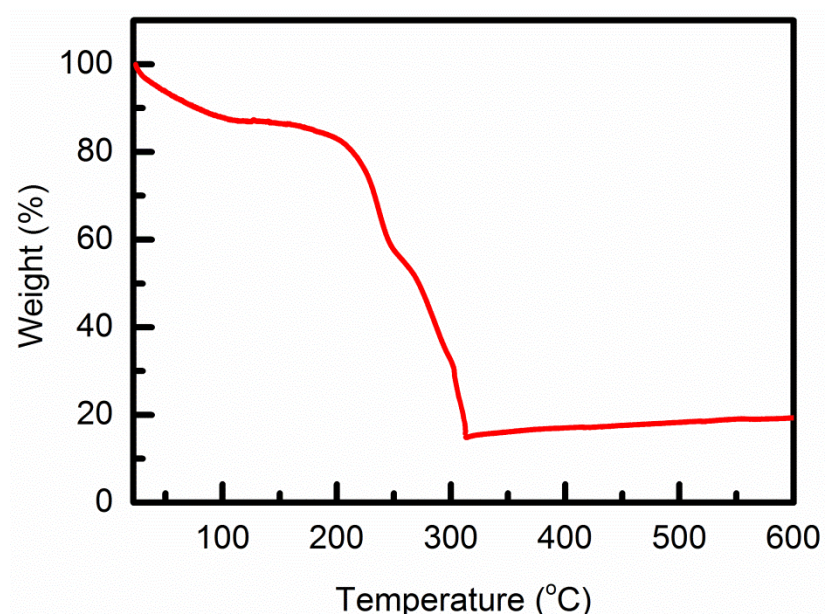
Figure S2. TGA curves of as–synthesized UTSA-200.
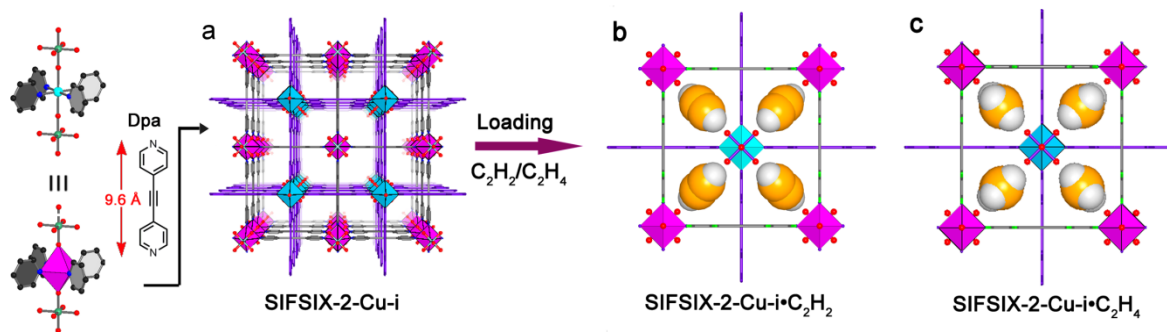
Figure S3. Structure description of SIFSIX-2-Cu-i. (**a**) The pore size channel structures in the diameter of 4.4 Å for SIFSIX-2-Cu-i viewed along the *c* axes. (**b, c**) DFT-D-calculated C_2H_2 (**b**) and C_2H_4 (**c**) adsorption models in SiFSIX-2-Cu-i viewed along the *c* axis, indicating that the pore size can allow the passage of both C_2H_2 and C_2H_2 molecules. The different nets are highlighted in gray and purple for clarity.
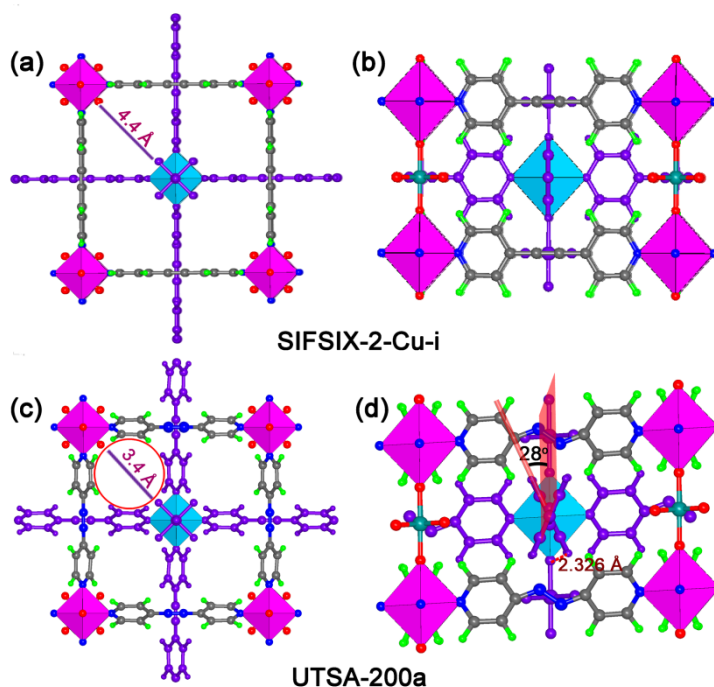
Figure S4. Structure description of SIFSIX-2-Cu-i (upper) and UTSA-200a (below), viewed along the *c* (**a, c**) and *b* (**c, d**) axes, respectively, showing a certain degree of titling of both of pyridine rings in UTSA-200a due to the flexibility nature of azpy molecule. The different net is highlighted in purple blue for clarity. Colour code: Cu (turquoise), Si (dark green), F (red), N (blue), C (grey), and H (green spheres).

(a) **(b)**

SIFSIX-2-Cu-i

(c) **(d)**

3.4 Å   4.6 Å
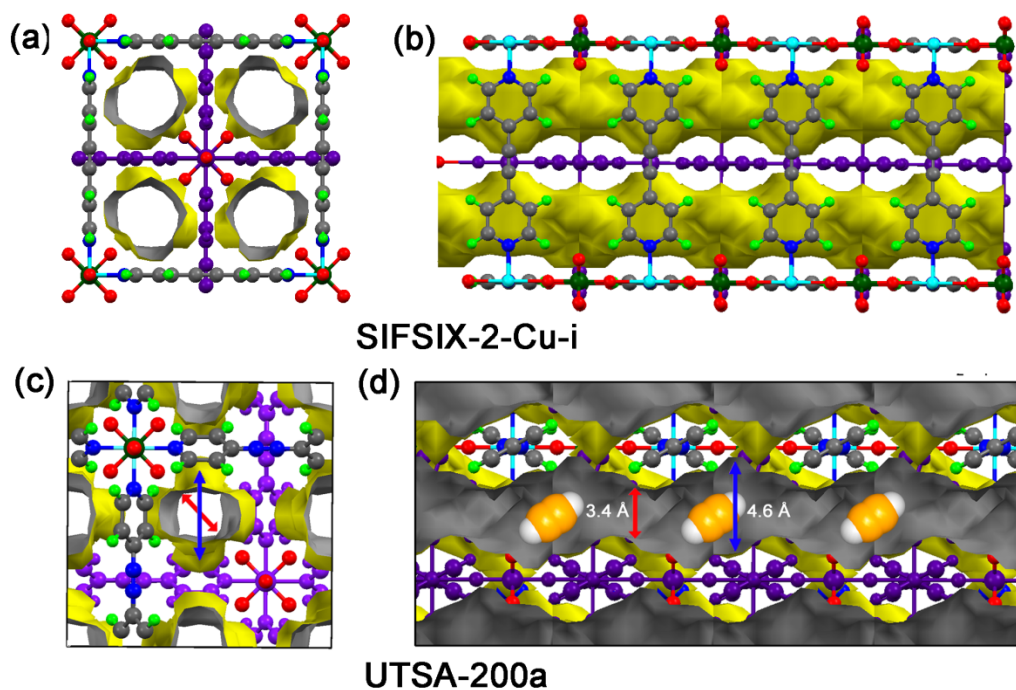
UTSA-200a

Figure S5. Solvent-accessible pore surface structure of SIFSIX-2-Cu-i and UTSA-200a: (**a**, **c**), viewed along the *c* axes; (**b**, **d**) and viewed along the *b* axes. Unlike the channel of SIFSIX-2-Cu-i, UTSA-200a shows the idealized pore channels as ideal molecular sieve, in which larger cavities in the diameter of about 4.6 Å are interconnected by very narrow apertures (molecular sieving dimension: ~3.4 Å). The different net is highlighted in dark blue for clarity. Colour code: Cu (turquoise), Si (dark green), F (red), N (blue), C (grey), and H (green spheres).
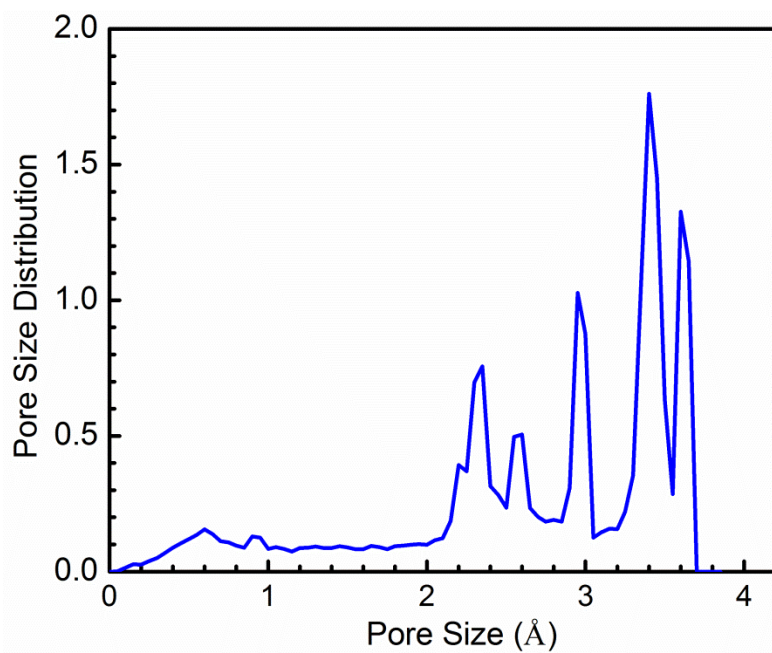
Figure S6. The calculated pore size distributions (PSD) of UTSA-200a. PSD was calculated using the well-known method by Gubbins et al.[18] The van der Waals diameters of the framework atoms were adopted from the Cambridge Crystallographic Center.
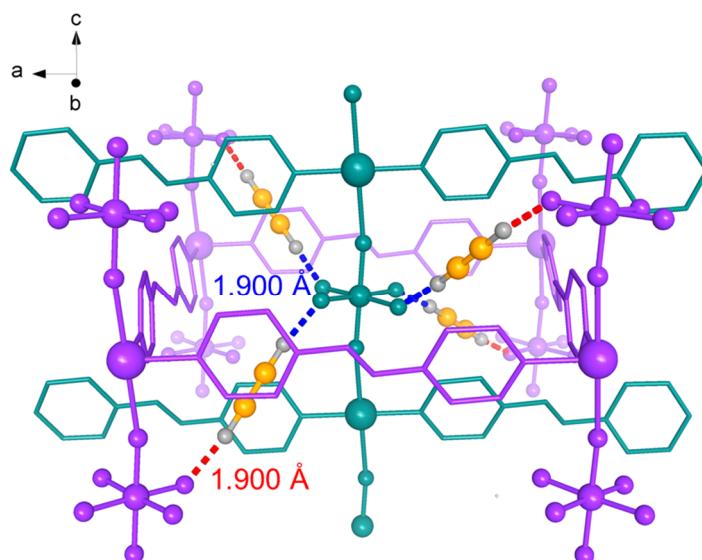
Figure S7. DFT-D–calculated C_2H_2 adsorption binding sites in UTSA-200a (the different nets are highlighted in purple and dark green for clarity). Color code: D, white; C (in C_2H_2) orange.
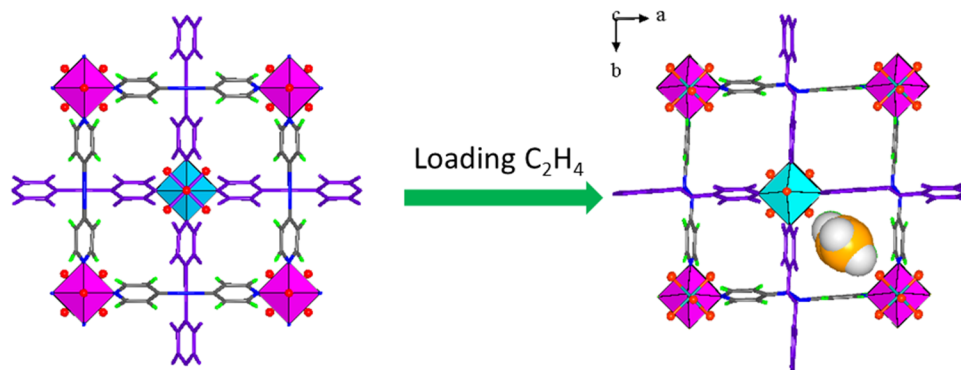
Figure S8. DFT-D-calculated C_2H_4 adsorption configuration in UTSA-200a (right structure), indicating that the N=N bond and pyridine rings on the azpy linker need to be rotated to make the dynamic pore size slightly larger under higher pressure (larger than 0.7 bar) to take up small amount of C_2H_4 gas molecules. The different net is highlighted in purple for clarity. Colour code: Cu (turquoise), Si (dark green), F (red), N (blue), C (grey), and H (green spheres).
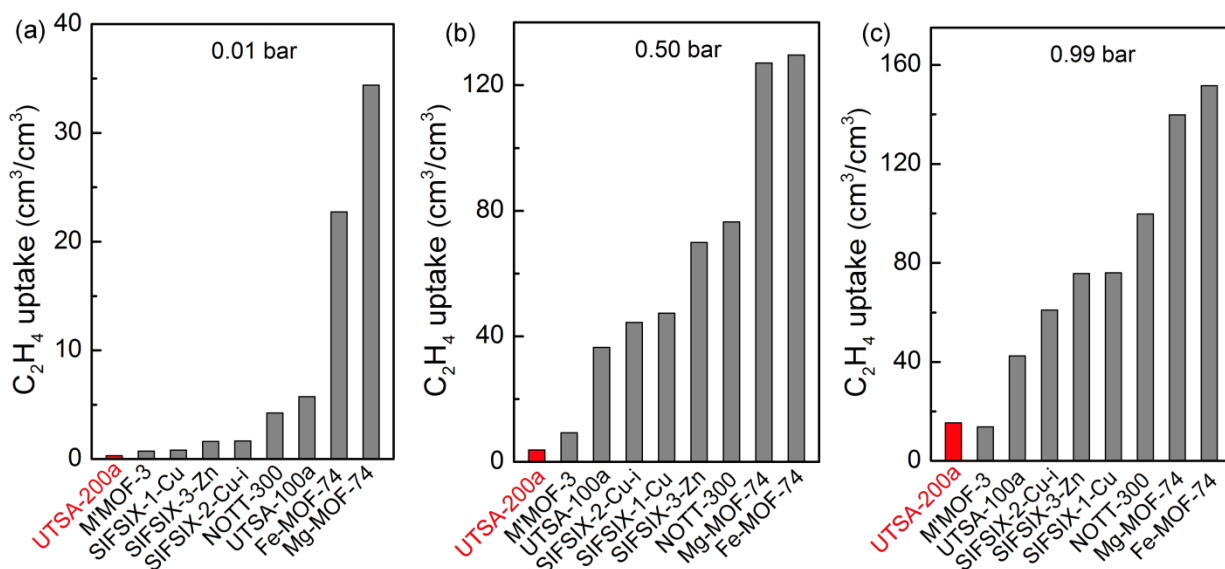
Figure S9. Comparison of C_2H_4 uptake (cm^3/cm^3) from gas sorption isotherms at various pressures for various MOF materials used in this study.
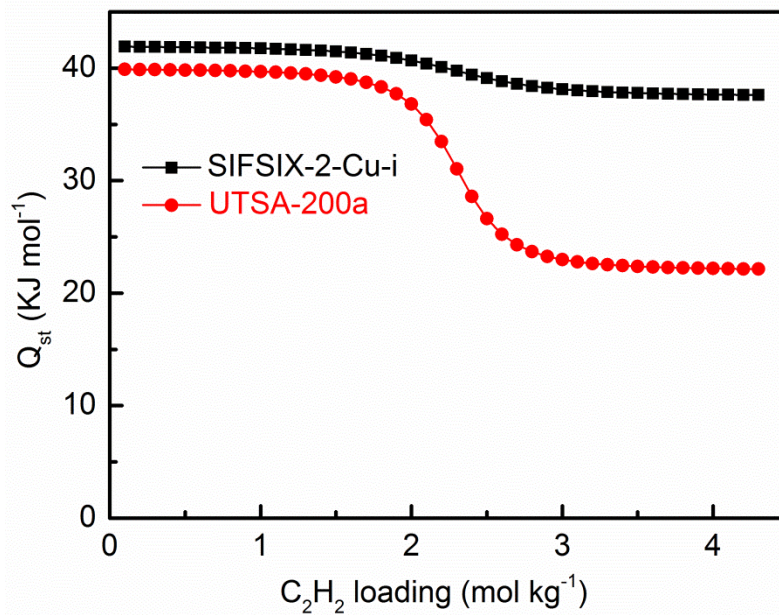
Figure S10. Comparison of Q_{st} of C_2H_2 adsorption in UTSA-200a and SIFSIX-2-Cu-i.
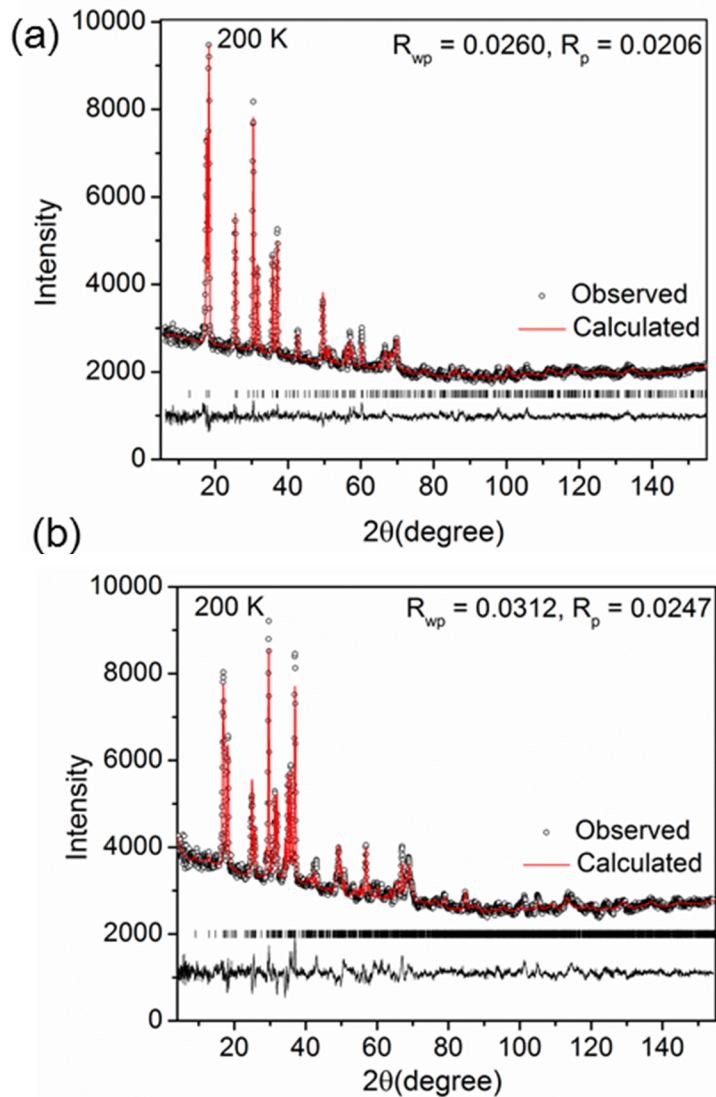
Figure S11. Neutron powder diffraction patterns for the Rietveld refinement of bare UTSA-200a (a) and C_2D_2-loaded UTSA-200a (b). Goodness of fit data: (a) $R_{wp}=0.0260$, $R_p=0.0206$; (b) $R_{wp}=0.0312$, $R_p=0.0247$.
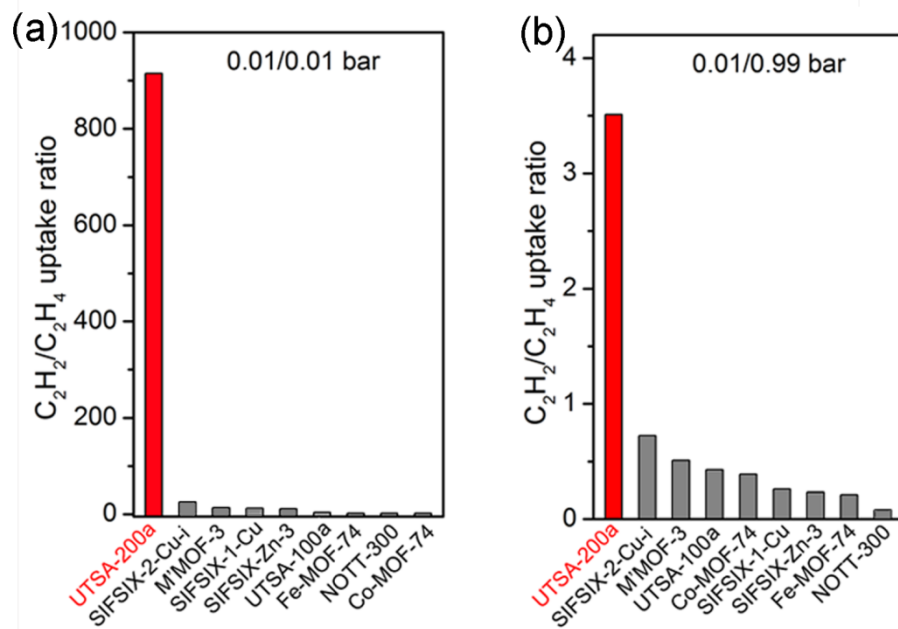
Figure S12. Comparison of C_2H_2/C_2H_4 uptake ratio at 0.01/0.01 bar (a) and 0.01/0.99 bar (b) for UTSA-200a with respect to other top-performing MOF materials as indicated.
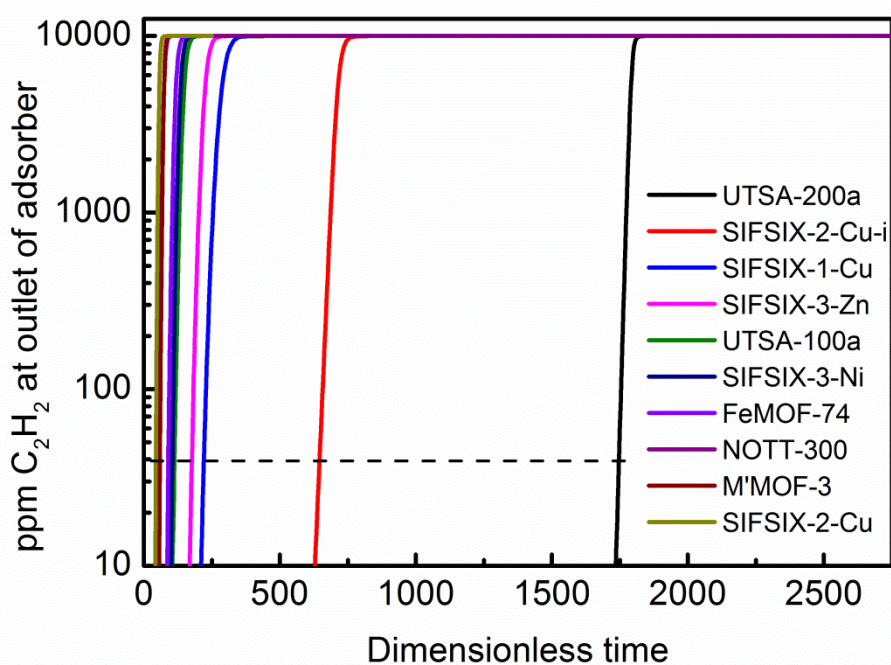
Figure S13. Ppm C_2H_2 in the outlet gas of transient breakthrough of C_2H_2/C_2H_4 mixture containing 1% C_2H_2 mixture in an adsorber bed packed with various MOFs. At a certain time, τ_{break}, the impurity level will exceed the desired purity level of 40 ppm.
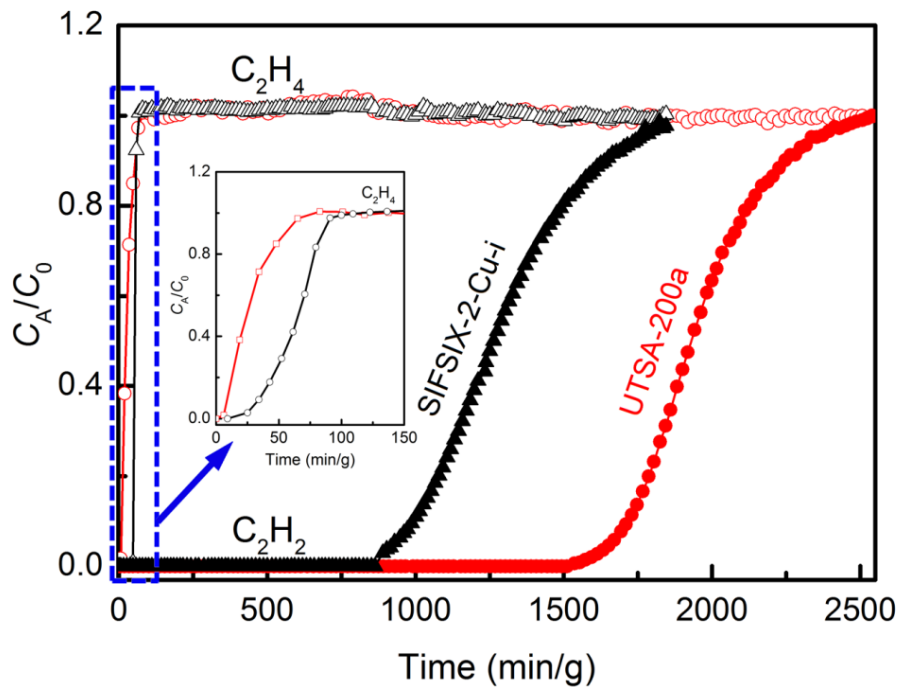
Figure S14. Experimental column breakthrough curves for C_2H_2/C_2H_4 (1/99, v/v) separation with UTSA-200a and SIFSIX-2-Cu-i at 298 K and 1.01 bar. The inset picture indicates that the C_2H_4 gas broke through the fixed UTSA-200a bed immediately due to the nearly fully molecular exclusion of C_2H_4 molecules, whereas the C_2H_4 gas passed through the fixed SIFSIX-2-Cu-i bed after a few minutes.
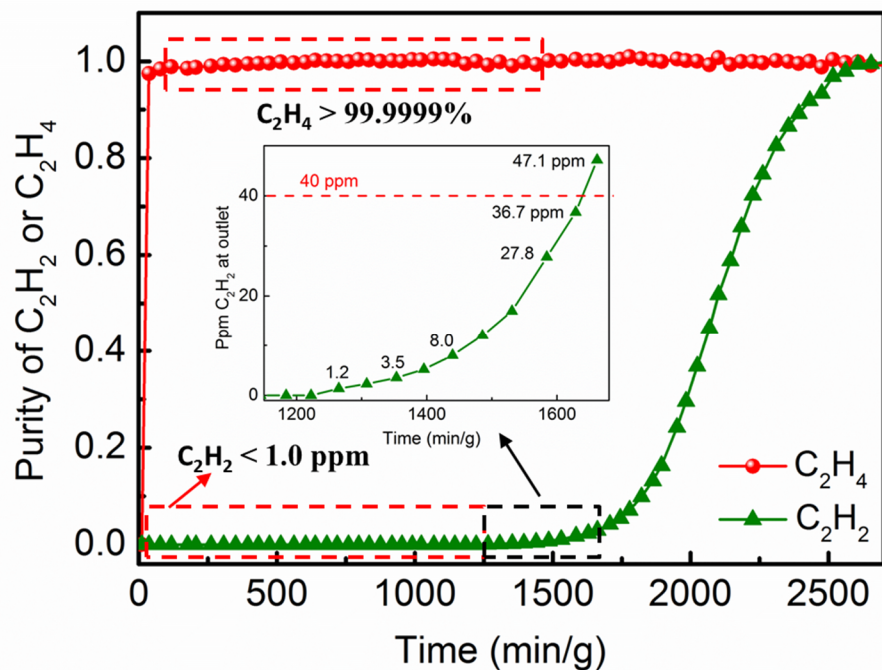
Figure S15. The concentration of C_2H_2 and the purity of C_2H_4 in the outlet gas of the adsorber. The inserted figure shows the C_2H_2 content in the outlet gas in ppm. Experimental breakthrough was conducted on a stainless steel column packed with UTSA-200a (4.6×50 mm) with C_2H_2/C_2H_4 mixture (1/99) as feed gas at 1.25 ml/min and 298 K.
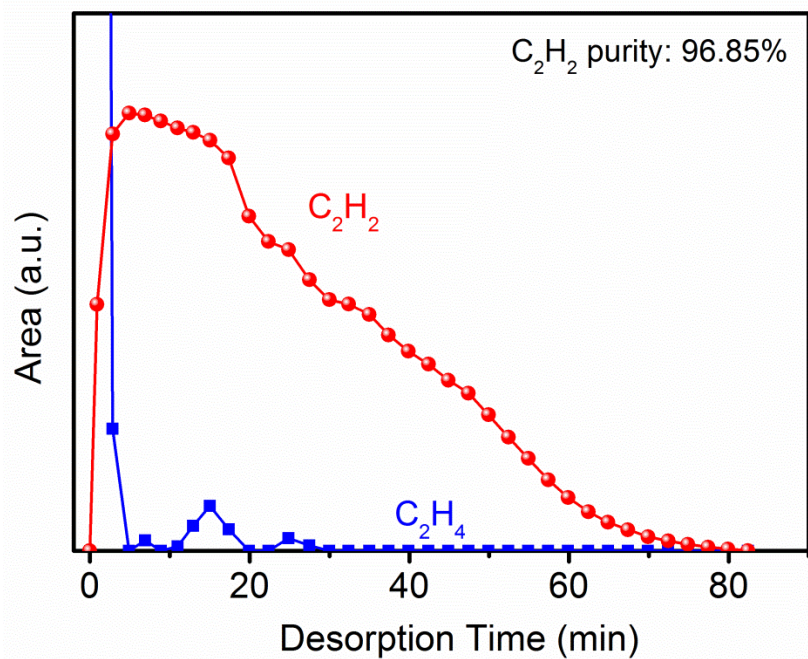
Figure S16. The signals of the desorbed C_2H_2 and C_2H_4 during regeneration process under flow of a 71.775/27.5/0.725 gas mixture of C_2H_4, N_2, and C_2H_2 at 338 K (Related to Experimental Procedures) at 338 K. The signal of C_2H_2 and C_2H_4 were processed with the subtraction of background signal. Nitrogen in the mixed gases was used to calibrate the change of the flow rate during desorption process.
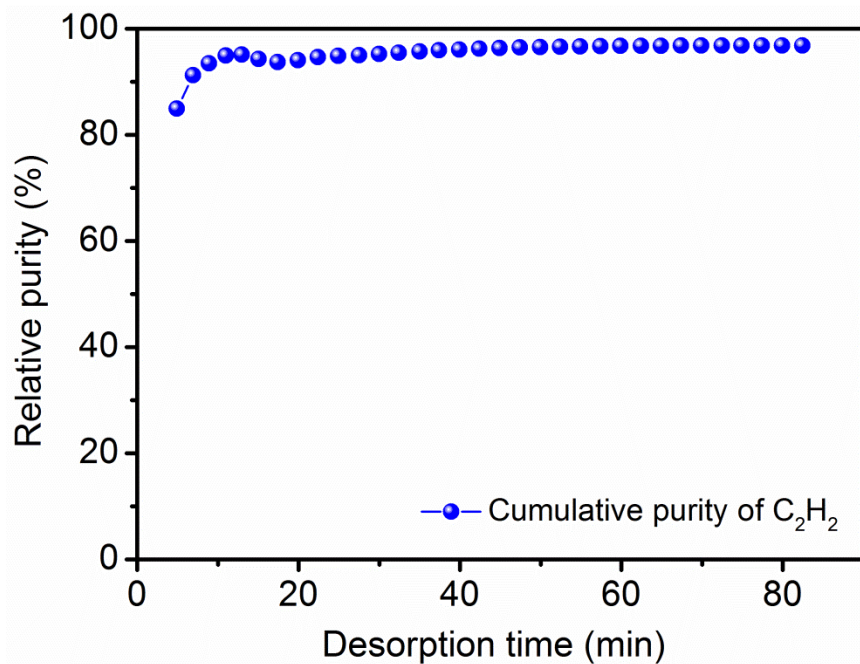
Figure S17. The calculated relative purity (cumulative) of desorbed C_2H_2 during desorption process at 338 K. This relative purity was calculated with the subtraction of background signal (inlet gas) and nitrogen content. Nitrogen in the mixed gases was used to calibrate the change of the flow rate during desorption process.
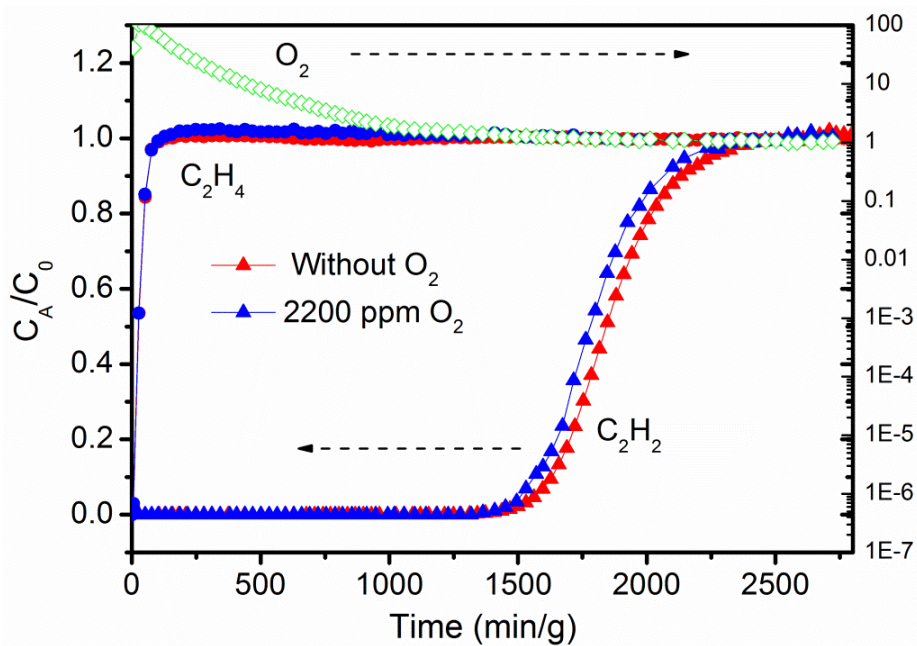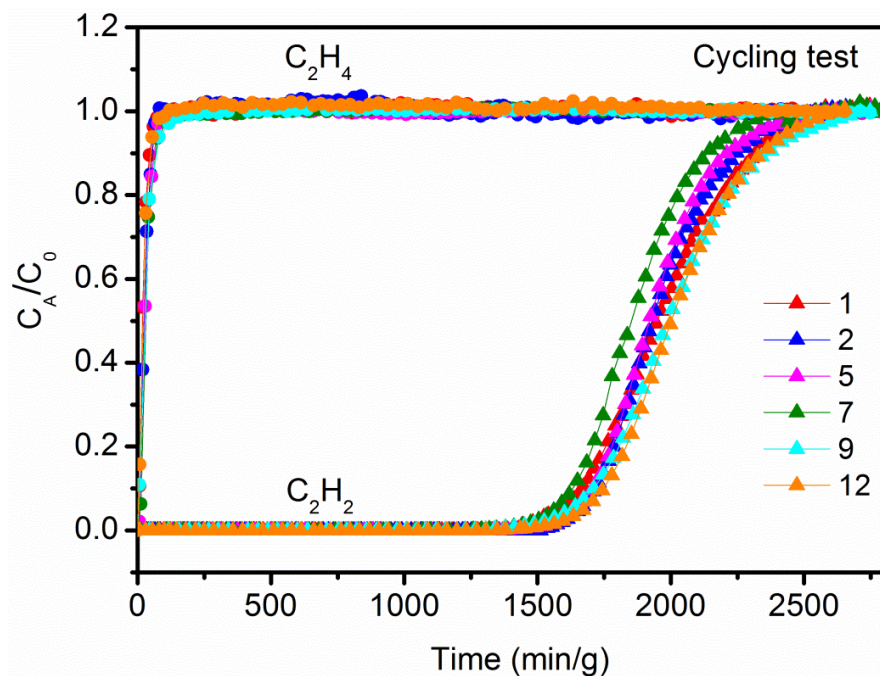
Figure S18. Experimental column breakthrough curves for C_2H_2/C_2H_4 separations (1/99, v/v) on UTSA-200a at 298 K and 1 bar with 2200 ppm O_2 and without O_2. The breakthrough experiments were carried out in a column packed with UTSA-200a (4.6 × 50 mm) at a flow rate of 1.25 ml/min.
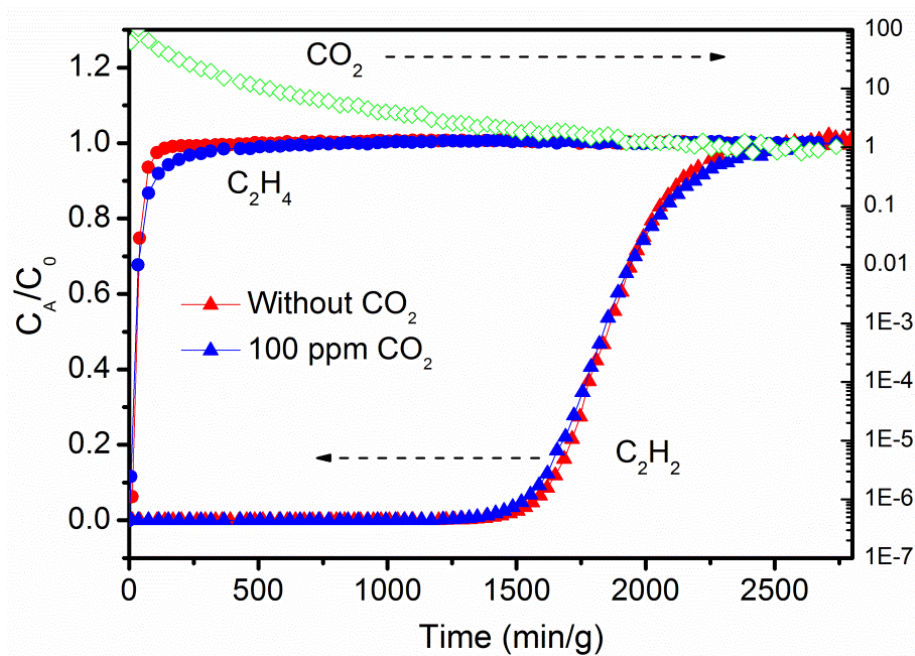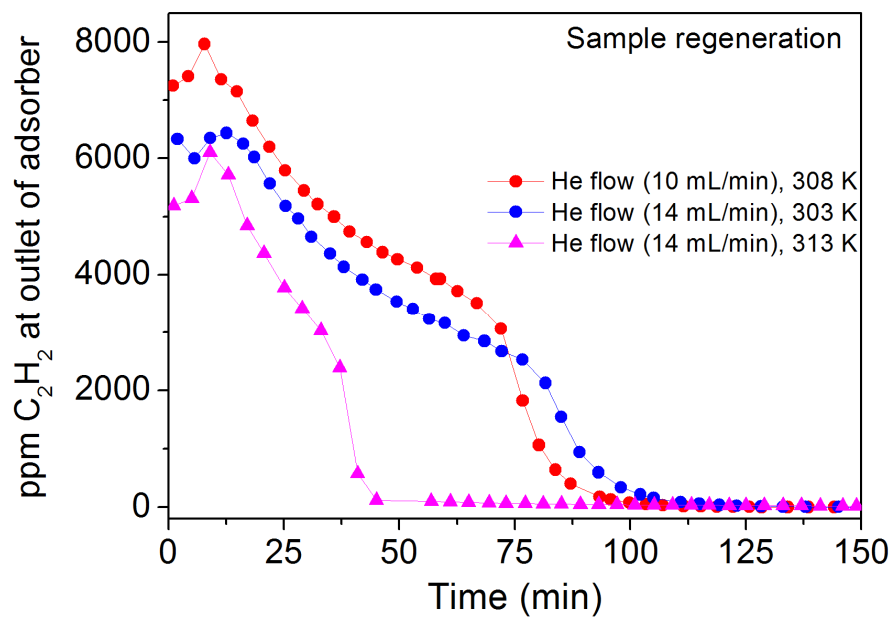
Figure S19. Experimental column breakthrough curves for C_2H_2/C_2H_4 (1/99, v/v) separations at 298 K and 1 bar in the absence and presence of 100 ppm CO_2. The breakthrough experiments were carried out in a column packed with UTSA-200a (4.6×50 mm) at a flow rate of 1.25 ml/min.
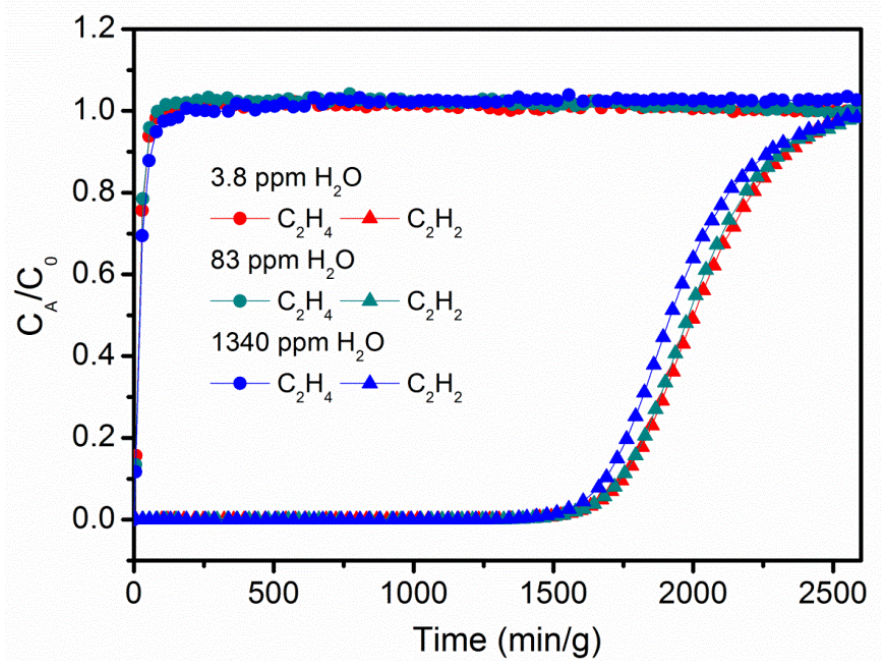
Figure S20. Experimental column breakthrough curves for C_2H_2/C_2H_4 separations (1/99, v/v) on UTSA-200a at 298 K and 1 atm with different amounts of H_2O. (1) 3.8 ppm H_2O, 1% C_2H_2 and 98.99% C_2H_4; (2) 83 ppm H_2O, 1% C_2H_2 and 98.99% C_2H_4; (3) 1340 ppm H_2O, 1% C_2H_2 and 98.86% C_2H_4. The breakthrough experiments were carried out in a column packed with UTSA-200a (4.6 × 50 mm) at a flow rate of 1.25 ml/min.

Figure S21. Cycling column breakthrough curves for C_2H_2/C_2H_4 separations (1/99, v/v) with UTSA-200a at 298 K and 1 bar. The breakthrough experiments were carried out in a column packed with UTSA-200a (4.6×50 mm) at a flow rate of 1.25 ml/min. Regeneration with He flow (7 to 15 mL/min) for 7 to 12 h at 308 or 313 K.

Figure S22. Experimental desorption curves for C_2H_2 at different temperatures and He flow rates. Before desorption, the breakthrough experiments for C_2H_2/C_2H_4 (1/99, v/v) mixture was carried out in a column packed with UTSA-200a (4.6×50 mm) at 298 K.
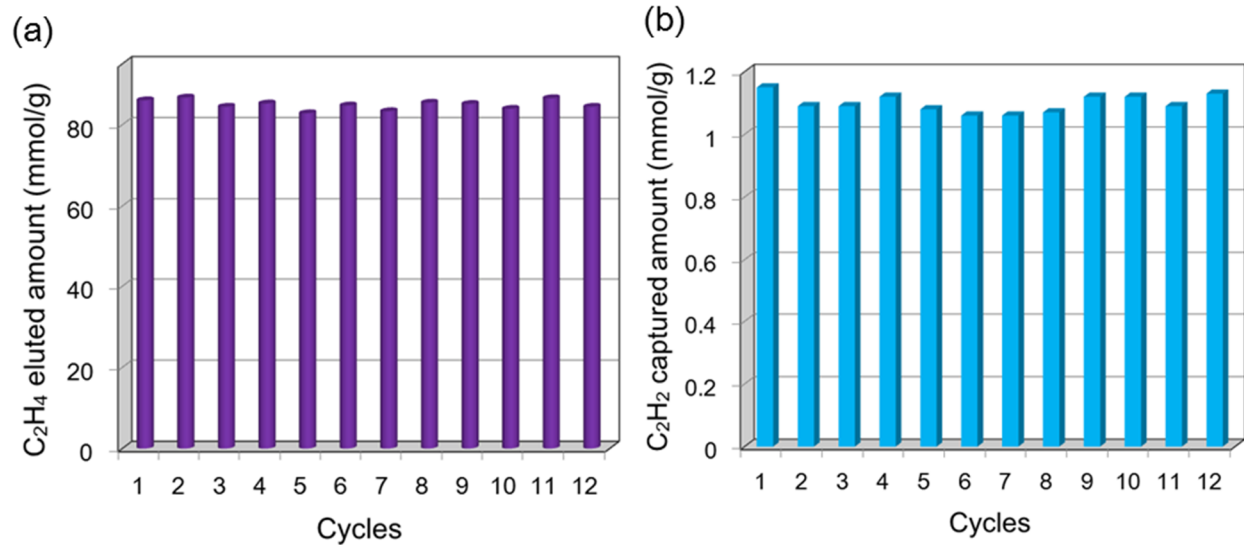
Figure S23. Cyclic breakthrough experiments on UTSA-200a at 298 K and 1 bar, indicating that UTSA-200a maintained the C_2H_4 eluted amount from the outlet effluent and the C_2H_2 captured amount during the separation processes over at least 12 times.
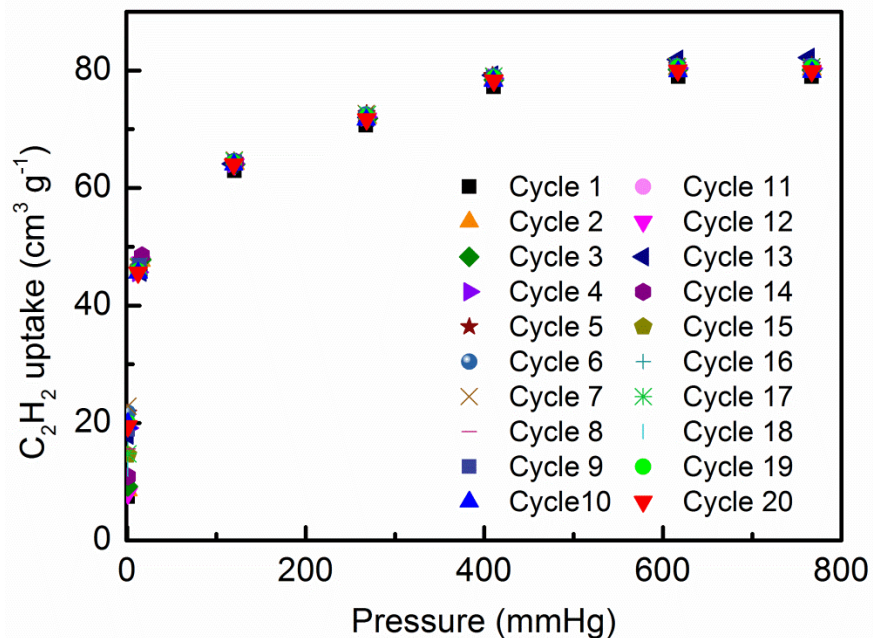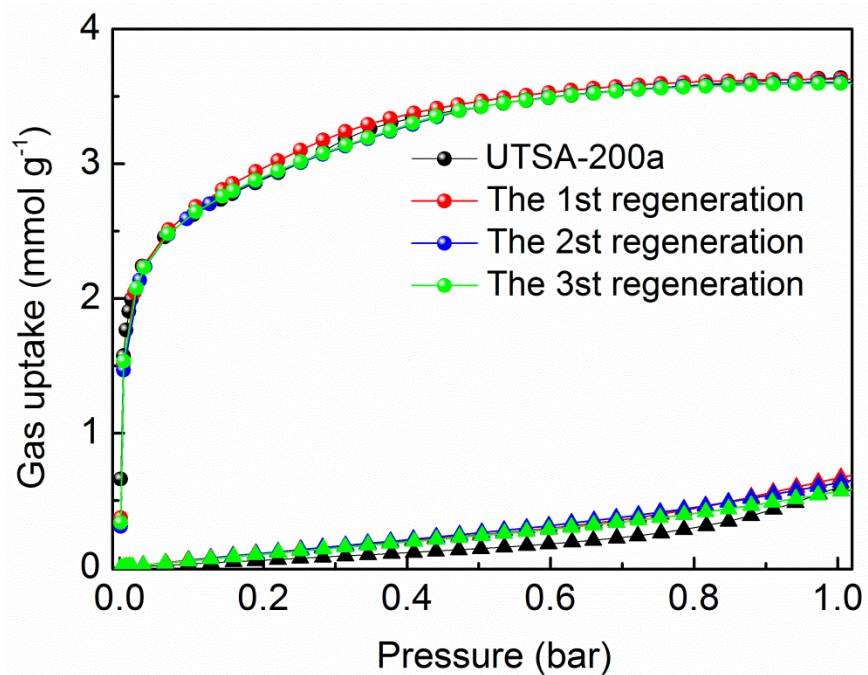
Figure S24. Cyclic C_2H_2 adsorption measurements on UTSA-200a at 298 K and 1 bar, indicating that UTSA-200a maintained its C_2H_2 uptake capacity over at least 20 times.
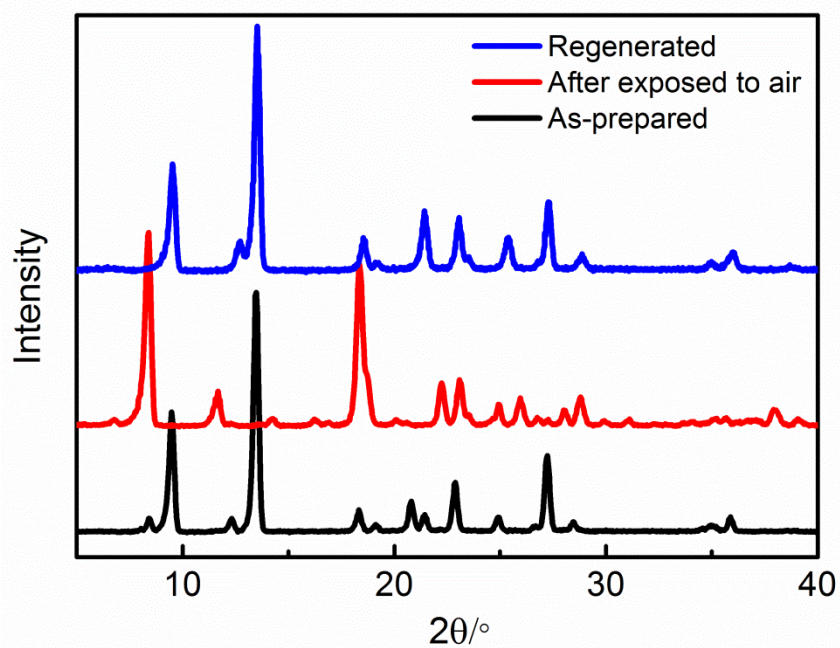
Figure S25. PXRD patterns of as-synthesized samples (black), the samples after exposed to air for two days (red), and the regenerated UTSA-200 (blue) in methanol solution.

Figure S26. C_2H_2 and C_2H_4 adsorption isotherms of UTSA-200a (red) and the regenerated sample after exposure to air (blue) over three cycles.
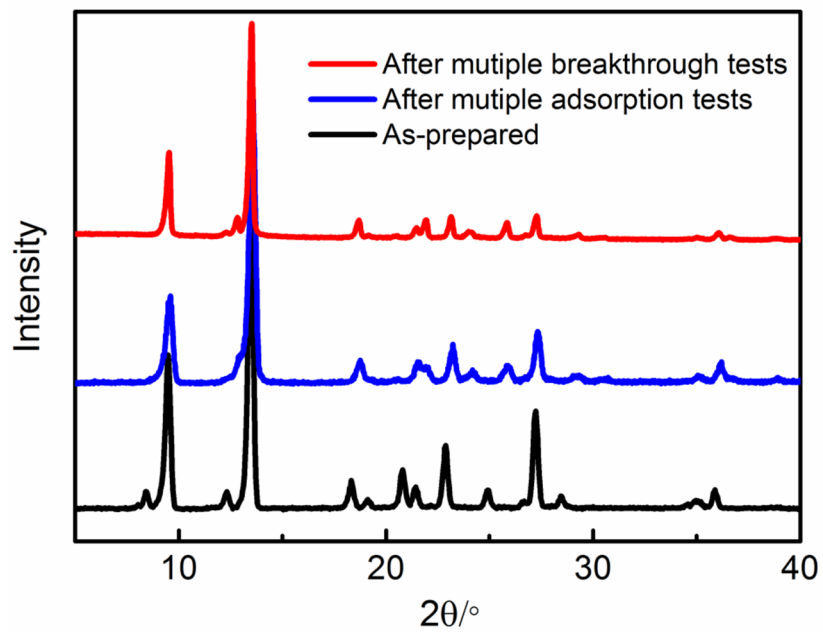
Figure S27. PXRD patterns of as-synthesized samples (black) and the samples after the multiple adsorption tests (blue) and breakthrough tests (red).

REFERENCES

[1] X. Cui, K. Chen, H. Xing, Q. Yang, R. Krishna, Z. Bao, H. Wu, W. Zhou, X. Dong, Y. Han, B. Li, Q. Ren, M. J. Zaworotko, B. Chen, *Science* **2016**, *353*, 141.

[2] K. M. Sundaram, M. M. Shreehan, E. F. Olszewski, *"Ethylene," in Kirk-Othmer Encyclopedia of Chemical Technology*, Wiley Online Library, **2001**.

[3] Bruker; Bruker AXS Inc.: Madison, Wisconsin, USA, **2010**.

[4] Bruker; Data Reduction Software. Bruker AXS Inc.: Madison, Wisconsin, USA, **2009**.

[5] G. M. Sheldrick, *Program for empirical absorption correction: University of Göttingen, Göttingen*, Germany, **2008**.

[6] A. Altomare, G. Cascarano, C. Giacovazzo, A. Guagliardi, *J. Appl. Crystallogr.* **1994**, *27*, 435.

[7] G. M. Sheldrick, *Acta Crystallogr., Sect. A: Found. Crystallogr.* **2008**, *64*, 112.

[8] A. L. Spek, *J. Appl. Crystallogr.* **2003**, *36*, 7.

[9] A. C. Larson, R. B. V. Dreele, General Structure Analysis System (LAUR 86-748, Los Alamos National Laboratory, 1994).

[10] V. Barone, M. Casarin, D. Forrer, M. Pavone, M. Sambi, A. Vittanini, *Comput. Chem.* **2009**, *30*, 934.

[11] T.-L. Hu, H. Wang, B. Li, R. Krishna, H. Wu, W. Zhou, Y. Zhao, Y. Han, X. Wang, W. Zhu, Z. Yao, S. Xiang, B. Chen, *Nat. Commun.* **2015**, *6*, 7328.

[12] R. Krishna, *Microporous Mesoporous Mater.* **2014**, *185*, 30.

[13] R. Krishna, *RSC Adv.* **2015**, *5*, 52269.

[14] Y. He, R. Krishna, B. Chen, *Energy Environ. Sci.* **2012**, *5*, 9107.

[15] S. Yang, A. J. Ramirez-Cuesta, R. Newby, V. Garcia-Sakai, P. Manuel, S. K. Callear, S. I. Campbell, C. C. Tang, M. Schröder, *Nat. Chem.* **2014**, *7*, 121.

[16] E. D. Bloch, W. L. Queen, R. Krishna, J. M. Zadrozny, C. M. Brown, J. R. Long, *Science* **2012**, *335*, 1606.

[17] S.-C. Xiang, Z. Zhang, C.-G. Zhao, K. Hong, X. Zhao, D.-R. Ding, M.-H. Xie, C.-D. Wu, M. C. Das, R. Gill, K. M. Thomas, B. Chen, *Nat. Commun.* **2011**, *2*, 204.

[18] S. Bhattacharya, K. E. Gubbins, *Langmuir* **2006**, *22*, 7726.